

Optical Spectroscopy of GRO J1655–40

Roberto Soria¹, Kinwah Wu², Richard W. Hunstead³

ABSTRACT

We have obtained optical spectra of the soft X-ray transient GRO J1655–40 during different X-ray spectral states (quiescence, high-soft and hard outburst) between 1994 August and 1997 June. Characteristic features observed during the 1996–97 high-soft state were: a) broad absorption lines at $H\alpha$ and $H\beta$, probably formed in the inner disk; b) double-peaked He II $\lambda 4686$ emission lines, formed in a temperature-inversion layer on the disk surface, created by the soft X-ray irradiation; c) double-peaked $H\alpha$ emission, with a strength associated with the hard X-ray flux, suggesting that it was probably emitted from deeper layers than He II $\lambda 4686$. The He II $\lambda 4686$ line profile appeared approximately symmetric, as we would expect from a disk surface with an axisymmetric emissivity function. The Balmer emission, on the other hand, appeared to come only from a double-armed region on the disk, possibly the locations of tidal density waves or spiral shocks. The observed rotational velocities of all the double-peaked lines suggest that the disk was extended slightly beyond its tidal radius.

Three classes of lines were identified in the spectra taken in 1994 August–September, during a period of low X-ray activity between two strong X-ray flares: broad absorption, broad (flat-topped) emission and narrow emission. We have found that the narrow (single-peaked or double-peaked) emission lines cannot be explained by a conventional thin accretion disk model. We propose that the system was in a transient state, in which the accretion disk might have had an extended optically thin cocoon and significant matter outflow, which would also explain the systematic blue-shift of the narrow emission lines and the flat-topped profiles of the broad emission lines.

After the onset of a hard X-ray flare the disk signatures disappeared, and strong single-peaked $H\alpha$ and Paschen emission was detected, suggesting that the cocoon became opaque to optical radiation. High-ionization lines disappeared or weakened. Two weeks after the end of the flare, the cocoon appeared to be once again optically thin.

Subject headings: accretion, accretion disks – binaries: spectroscopic – black hole physics – stars: individual (GRO J1655–40)

¹Research School of Astronomy and Astrophysics, Australian National University, Private Bag, Weston Creek Post Office, ACT 2611, Australia; roberto@mso.anu.edu.au

²Research Centre for Theoretical Astrophysics, School of Physics, University of Sydney, NSW 2006, Australia

³Department of Astrophysics, School of Physics, University of Sydney, NSW 2006, Australia

1. INTRODUCTION

Among the low-mass X-ray binaries, soft X-ray transients (SXTs) offer a favorable opportunity of detecting stellar-mass black-hole candidates (BHCs). Measurements of the binary periods and the orbital velocities of the companion stars in seven SXTs yield mass functions $\gtrsim 3M_{\odot}$ for their compact stars (McClintock 1998, Filippenko et al. 1999). As these masses are higher than the upper limit to the mass of neutron stars for known equations of state of nucleon matter, the compact stars in SXTs are all BHCs. In other two systems, the mass functions are $< 3M_{\odot}$ but the inclination angles are thought to be sufficiently low that the compact objects can also be classified as BHCs (McClintock 1998).

SXTs show transitions between different spectral states. In a simple classification, we can identify an “off” (or “quiescent”) state when the source is inactive, and a “high-soft state” and a “low-hard state” defined by their X-ray spectral properties, when the source is X-ray active. Often an increase of the optical brightness and radio flares accompany the X-ray outbursts. (See e.g. Tanaka & Lewin 1995 for a review of the properties of SXTs.)

GRO J1655–40 is an SXT discovered by BATSE on 1994 July 27 (Zhang et al. 1994). Between 1994 and 1995 it underwent several X-ray outbursts (see Tavani et al. 1996), after which it retreated to a quiescent state. In late April 1996, another outburst started, and it lasted more than one year. The 2 – 12 keV X-ray light curve of GRO J1655–40 during the 1996 outburst is shown in Figure 1 (from the quick-look results provided by the RXTE/ASM team); in the same figure we also show the hard (20 – 100 keV) X-ray flux detected by BATSE over the same period of time.

The binary period of GRO J1655–40 is $P = 2.62157 \pm 0.00015$ d (Orosz & Bailyn 1997). The time of inferior conjunction of the secondary star is HJD 2449838.4209 \pm 0.0055 (Orosz & Bailyn 1997). An alternative ephemeris, given by van der Hooft et al. (1998), is HJD 2449838.4198(52) + 2.62168(14) \times N.

The mass function determined from the kinematics of the system by Orosz & Bailyn (1997) implies a mass $M_1 = (7.0 \pm 0.2) M_{\odot}$ for the compact object. By taking into account the effect of X-ray irradiation of the secondary star, Phillips, Shahbaz & Podsiadlowski (1999) derived lower values for the mass of the primary: they obtained $4.1 < M_1 < 6.6M_{\odot}$ (90 per cent confidence level). By using only data taken during an X-ray quiescent state, Shahbaz et al. (1999) obtained $5.5 < M_1 < 7.9M_{\odot}$ (95 per cent confidence level). In any case, the mass of the compact object makes GRO J1655–40 a candidate black hole binary. The major orbital parameters of the system are listed in Table 1.

During the quiescent states the system is optically faint, with $V \approx 17$ mag (Bailyn et al. 1995b), but it can brighten substantially when an X-ray outburst occurs. In August 1994, it reached $V = 14.4$ (Bailyn et al. 1995a), and in May 1996, $V = 15.4$ (Horne et al. 1996).

Since its discovery, we have observed GRO J1655–40 spectroscopically on four occasions: 1994 August – September, 1996 April, 1996 June and 1997 June. The observations covered periods in

which the system was in a pre-outburst quiescence, at the onset of a hard X-ray flare and in a high-soft state. In a previous paper (Soria et al. 1998) we presented the orbital-phase-dependent velocity shifts of the He II $\lambda 4686$ and N III $\lambda\lambda 4641, 4642$ emission lines.

In this paper we extend our study to include the Balmer lines and the orbital variations in their line profiles. Technical details of our observations are outlined in §2. In §3 we present the results of the spectroscopic observations we conducted in 1996 April, and in §4 we present those we obtained in 1996 June and 1997 June. In §5 we discuss the profiles of the Balmer lines observed in the 1996 – 1997 soft X-ray outburst, and we attempt to locate the emission regions. We also discuss some physical mechanisms responsible for line emission and absorption in the disk. In §6 we present the results of the observations we carried out during the 1994 hard X-ray outburst. We outline the general spectral features, we discuss the origin, intensity and profile of the main absorption and emission lines, and we compare the two sets of spectra from 1994 and 1996. In particular, we show the evolution of the optical spectrum before, during and after a major hard X-ray flare.

2. OBSERVATIONS

GRO J1655–40 was observed by one of us (RWH) as a target of opportunity on each night from 1994 August 30 to 1994 September 4, with the RGO spectrograph and Tektronix $1k \times 1k$ thinned CCD on the 3.9 m Anglo-Australian Telescope (AAT). Spectra were obtained in two regions, $6278 - 6825 \text{ \AA}$, centered on the $H\alpha$ line, and $4432 - 5051 \text{ \AA}$, covering the N III, He II and $H\beta$ lines. Gratings with 1200 grooves/mm were used, with the blaze direction oriented towards the 25 cm camera, giving a resolution of 1.3 \AA FWHM. On September 6, we obtained simultaneously a blue ($3925 - 5500 \text{ \AA}$) spectrum with the RGO spectrograph and 600 grooves/mm gratings, at a resolution of 2.5 \AA FWHM, and a red ($5500 - 11000 \text{ \AA}$) spectrum with the FORS spectrograph, via a dichroic beam splitter, at a resolution of 20 \AA FWHM. The latter observations were kindly obtained for us by Paul Francis.

In 1996 April 20 – 21 we carried out a scheduled observation with the Double Beam Spectrograph (DBS) on the ANU 2.3 m Telescope at Siding Spring Observatory. The detectors on the two arms of the spectrograph were SITE 1752×532 CCDs. Gratings with 300 grooves/mm were used for the blue ($3600 - 5700 \text{ \AA}$) and the red ($5700 - 9300 \text{ \AA}$) bands, and low-resolution spectra (resolution = 4.8 \AA FWHM) were obtained. More extensive observations were carried out in 1996 June 8 – 12 and June 17, and 1997 June 14 – 15, with the DBS on the ANU 2.3 m Telescope. 1200 grooves/mm gratings were used for both the blue ($4150 - 5115 \text{ \AA}$) and the red ($6300 - 7250 \text{ \AA}$) bands, giving a resolution of 1.3 \AA FWHM. We list our observations in Table 2.

3. PRE-OUTBURST STATE (1996 APRIL)

3.1. Overview

GRO J1655–40 was in quiescence between late 1995 August and 1996 April. In 1996 March, its soft X-ray luminosity, inferred from the ASCA observations (at 2 – 10 keV), was $\approx 2 \times 10^{32}$ erg s^{-1} (see Orosz & Bailyn 1997). The source was not detected by RXTE/ASM (at 2 – 12 keV) above the intensity level of ≈ 12 mCrab before 1996 April 25 (Levine et al. 1996; Remillard et al. 1996); it was also undetected by BATSE before May. On April 25.38 ± 0.78 UT (HJD 2450198.88 ± 0.78), the soft (2 – 12 keV) X-ray intensity began to rise (Remillard et al. 1996). The optical brightening, however, had already started on April 20 (Orosz et al. 1997). The fitted times of the initial rise were April 19.25 ± 0.29 UT (HJD 2450192.76 ± 0.29) for the *I* band, April 19.37 ± 0.26 UT (HJD 2450192.88 ± 0.26) for the *R* band, April 19.82 ± 0.15 UT (HJD 2450193.32 ± 0.15) for the *V* band and April 20.34 ± 0.18 UT (HJD 2450193.84 ± 0.18) for the *B* band.

Our spectroscopic observations were conducted between HJD 2450194.26 and HJD 2450194.30 (April 20), and between HJD 2450195.10 and HJD 2450195.15 (April 21), just after the initial rise in the optical brightness, but before the RXTE/ASM detected the rise in the X-ray intensity. On the first night we took a series of five 600-s spectra and one 1200-s spectrum (although focussing problems on the red arm of the spectrograph affected the quality our red spectra). The binary phase during the observations was $0.485 < \phi < 0.501$ (ephemeris of Orosz & Bailyn 1997), and the inferior conjunction of the secondary star was at $\phi = 0.75$. On the following night, we took seven 600-s spectra, at the binary phase $0.804 < \phi < 0.824$. (If we adopt the ephemeris of van der Hooft et al. (1998), the observations were made at phase $0.480 < \phi < 0.496$ on the first night, and $0.799 < \phi < 0.819$ on the second.)

3.2. General spectral features

The H I Balmer and Paschen lines are clearly seen in absorption in our spectra (Figures 2 and 3). The He II $\lambda 4686$ emission line, the Bowen fluorescence N III $\lambda 4634$ line and the blend N III $\lambda\lambda 4641, 4642$ were not detected on either night. These emission lines, which are often seen from X-ray irradiated accretion disks (Smak 1981; Horne & Marsh 1986), were, however, observed 20 days later (on May 11) by Hynes et al. (1998b).

By comparing our spectra with the spectra of F giant and subgiant stars and with the spectra of the system taken by Orosz & Bailyn (1997) during a quiescent state in February 1996, we conclude that the optical continuum emission was predominantly from the secondary star. This conclusion is supported by the agreement between the observed velocity shifts of the Balmer lines in our spectra and the radial velocity of the secondary star expected at those phases (not shown).

4. HIGH-SOFT STATE (1996–1997)

4.1. 1996 June observations

In late 1996 April, a transition from quiescence to a high/soft X-ray state occurred. The soft (2 – 12 keV) X-ray flux (measured by RXTE/ASM) increased rapidly, reaching $\gtrsim 1.5$ Crab and remaining above that level for more than six months. Around 1996 November the soft X-ray intensity began to decline; but in 1997 January it increased again (Figure 1). It then stayed at the ≈ 1.3 Crab level till 1997 July, after which the system entered another quiescent state.

At the initial stage of the outburst the X-ray spectrum consisted of a blackbody component and a truncated power-law tail. The black body temperature was $T \simeq 0.8$ keV. The photon index of the power-law tail was $\Gamma \simeq 3.5$ and the exponential cutoff was at $\simeq 13$ keV (Hynes et al. 1998b). Around 1996 May 27 – 28 (HJD 2450230 – 31) the X-ray spectrum hardened, and the source became detectable by BATSE (Figure 1). The photon index of the power-law was $\Gamma \simeq 2.5$ on June 20, and there was no obvious sign of a high-energy cutoff below $\simeq 100$ keV (Hynes et al. 1998b). A radio flare was observed by the Molongo Observatory Synthesis Telescope (MOST), apparently coincident the X-ray spectral transition (Hunstead & Campbell-Wilson 1996; Hunstead, Wu & Campbell-Wilson 1997).

The optical continuum had increased a few days before the onset of the soft X-ray outburst (see §3.1). After reaching a peak in mid-May, the optical brightness then declined steadily, with an e-folding time of about 50 days (Hynes et al. 1998b). By August 1996 it had returned to the previous quiescent level. Flickerings on time-scales of a few seconds, apparently correlated with X-ray variability, were reported by Hynes et al. (1998a).

Our observations were carried out on June 8 – 12 and June 17, during the soft X-ray outburst (Figure 1). We obtained fifty simultaneous red and blue spectra, each of 2000 s duration. In Figure 4 we show two blue and red spectra taken on June 8 and June 10. The intensity of the optical continuum in May was slightly higher than in June (cf. Hynes et al. 1998b). The soft X-ray flux was similar in these two epochs; however, the hard X-rays turned on after May 27.

4.2. General spectral features in the 1996 June observations

The $H\alpha$ and $H\beta$ lines showed a broad absorption trough in 1996 June. The absorption component was stronger on June 8 (EW $\simeq -6$ Å, FWHM $\simeq 70$ Å $\simeq 3000$ km s $^{-1}$ for $H\alpha$; EW $\simeq -10$ Å, FWHM $\simeq 70$ Å $\simeq 4000$ km s $^{-1}$ for $H\beta$) than on the other nights. The absorption troughs were partly filled by narrower emission components (Figure 4), which were not seen in the spectra obtained by Hynes et al. (1998b) four weeks earlier.

The equivalent width of the $H\alpha$ emission seemed to increase with the hard X-ray flux (Figure 5). The emergence of the $H\alpha$ emission component after the May 27 turn-on of the hard X-ray flux also

suggests a direct association between these emissions. We have calculated the discrete correlation function, defined by Edelson & Krolik (1988), for the EW of the H α emission line and the hard X-ray flux and have found a 2- σ peak in the correlation function at the lag of 0.0 ± 0.5 d, for a 0.5 d interval bin (Figure 6). A similar correlation is also found in our 1994 August – September data (see §6.4.1).

The average H α emission profile was double-peaked, with FWHM $\simeq 900$ km s $^{-1}$, and peak-to-peak velocity separation = 500 ± 50 km s $^{-1}$. However, the relative strength of the two peaks varied substantially over each orbital cycle (see §4.3).

The He II $\lambda 4686$ emission line had a double-peaked profile (Figure 7) with a peak-to-peak separation of 8.5 ± 0.5 Å, corresponding to a velocity separation of 545 ± 30 km s $^{-1}$. A double-peaked He II $\lambda 4686$ emission line had been detected before the X-ray hardening (see Table 6 in Hynes et al. 1998b): archival spectra from the Anglo-Australian Telescope show that the peak-to-peak velocity separation was 480 ± 40 km s $^{-1}$ on 1996 May 11. The central position of the line varied sinusoidally, with the variations consistent with the projected radial velocity of the primary star for a mass ratio $q = 0.33$ (Soria et al. 1998), suggesting that the emission originated from the accretion disk. The average line center was blue-shifted by $40 \pm 10 \pm 5$ km s $^{-1}$ with respect to the systemic velocity determined by Orosz & Bailyn (1997), where the first source of error is in the determination of the line center, the second is the systematic error in the wavelength calibration. We have not found any significant correlation between the EW of the He II $\lambda 4686$ line and the hard X-ray flux (Figure 5).

The He I $\lambda 6678$ emission line appeared to be double-peaked, with only one peak visible at some orbital phases. The velocity separation, which was determined when the two peaks were present, varied between 520 and 650 km s $^{-1}$ over the time of our observations. These velocities are consistent with those of the H α and the He II $\lambda 4686$ lines. The EW of the line was about 0.7 Å.

A weak narrow absorption component was also detected at $\lambda 6678$ (not shown), superimposed on the broader, double-peaked emission component. The narrow absorption component was visible at most orbital phases and had an EW $\simeq -0.2$ Å and an FWHM $\simeq 4$ Å ($\simeq 170$ km s $^{-1}$). A similar narrow absorption component was also found at $\lambda 7065$.

The velocity shifts of the narrow absorption components of the He I lines were consistent with the projected radial velocity of the secondary star (Figure 8), suggesting that these lines were due to absorption near the secondary star. The apparent small discrepancy between the observed and predicted velocities may be due in part to the uncertainty in our measurement of the line position, in part to additional absorption by cold gas near the rim of the accretion disk or in the accretion stream, or to a non-uniform absorption by the photosphere of the secondary star, which was strongly irradiated on the side facing the primary.

We note that He I $\lambda 7065$ showed a stronger broad absorption component briefly on June 8, with EW $\simeq -1.8$ Å and FWHM $\simeq 35$ Å $\simeq 1500$ km s $^{-1}$. It disappeared later on the same night while the hard X-ray flux increased, and was not seen during the following nights (see Figure 4).

Narrow, single-peaked N III $\lambda 4634$ and N III $\lambda\lambda 4641, 4642$ Bowen fluorescence lines were observed in 1996 June. As these lines were also seen before the hard X-ray turned on [see the spectra taken by Hynes et al. (1998b) in 1996 May], they were probably uncorrelated with the hard X-ray flux. By comparing the Bowen line profiles and radial velocity shifts with those of the He II $\lambda 4686$ line, we conclude that the Bowen fluorescence lines and the He II line originated from different regions. Judging from the radial velocities shifts of the Bowen lines, Soria et al. (1998) suggest that they were emitted from a localized region in the outer accretion disk, possibly a hot spot in phase with the secondary star.

4.3. Profile of the H α emission component

Among the emission lines observed in 1996 June, the H α line had the highest signal-to-noise ratio. If we adopt a reddening $E(B - V) = 1.2$ (Hynes et al. 1998b), the inferred average flux for the H α emission line was $F_{\text{H}\alpha} \approx 5 \times 10^{-13} \text{ erg cm}^{-2} \text{ s}^{-1}$ (cf. $F_{\text{He II}} \approx 3 \times 10^{-13} \text{ erg cm}^{-2} \text{ s}^{-1}$ for the He II $\lambda 4686$ line). Although the EW of the H α line appeared to be correlated with the hard X-ray flux (Figure 5), we have found that the velocity profile of the line, with its peak normalized to unity, depended only on the binary phase.

The systematic variation of the H α emission line profiles over an orbital cycle can be seen in the sequence of profiles plotted in Figures 9, 10 and 11. The red-shifted peak was stronger than the blue-shifted peak between phase 0.25 and 0.85, with the blue-shifted peak dominating at other phases. By considering the averaged, normalized H α line profiles over the whole epoch of our observations (see Figure 2 in Soria et al. 1998), and the averaged profiles obtained between orbital phases 0.80 and 0.92 and between phases 0.19 and 0.28 (Figure 12), when the highest signal-to-noise ratio was achieved and both peaks had comparable strength, we deduce that the FWHM of the line was $\simeq 900 \text{ km s}^{-1}$, and the peak-to-peak velocity separation was $500 \pm 50 \text{ km s}^{-1}$. These values are similar to those determined for the double-peaked He I and He II emission lines.

In principle, symmetric double-peaked lines can be produced by an accretion disk (Smak 1981; Horne & Marsh 1986). As the H α line profile changed with a period equal to the binary period, this eliminates the possibility that the line asymmetry was due to a precession of the accretion disk, which should have a period longer than the binary period (e.g. Kumar 1986, Warner 1995). Neither could it be caused by the secondary star eclipsing either side of the disk, because our data show asymmetry of the two peaks even when the star was behind the accretion disk.

If the emission were from the irradiatively-heated surface of the secondary star, we would expect a stronger blue component in the emission line when the star was approaching (at phases 0.25 — 0.75), and vice versa. This is inconsistent with the observation that the blue peak of the line was stronger at around phase 0. Therefore we reject the possibility that the secondary star was the dominant source of the emission. (See §5 for more detailed discussion on the H α emission.)

4.4. 1997 June observations

The soft X-ray flux in 1997 June was slightly lower than in 1996 June, while the hard X-ray flux was significantly lower (Figure 1). We observed the system on 1997 June 14 and 15. No optical photometric observations were carried out during this period. Although the conditions were not photometric, a comparison with other stars in the field led to an estimate of $V \gtrsim 16.5$ for the source, about half a magnitude fainter than in 1996 June.

The $H\alpha$ emission line had a red-shifted peak around phase 0.5 and a blue-shifted peak around phase 0, as in 1996 June; the signal-to-noise ratio was much lower than in 1996. The velocity shifts with respect to the center of mass of the binary were $\simeq 255 \text{ km s}^{-1}$ for the red-shifted peak, and $\simeq -230 \text{ km s}^{-1}$ for the blue-shifted peak, similar to those measured in 1996.

For the $H\alpha$ line, $EW = 2.5 \pm 0.4 \text{ \AA}$ on June 14, and $2.7 \pm 0.3 \text{ \AA}$ on June 15. The emission component of the $H\beta$ and higher Balmer lines was not detectable. The Balmer emission was therefore weaker than in 1996 June. The He II $\lambda 4686$ line was seen in emission with $EW = 3 \pm 1 \text{ \AA}$, as strong as in 1996. The Bowen fluorescence N III lines were also detected.

5. BALMER EMISSION IN THE HIGH-SOFT STATE

5.1. Kinematic interpretation of the $H\alpha$ emission

5.1.1. Peak separation

Figure 13 shows the velocity shift of the peaks of the $H\alpha$ emission component detected in the 1996 June and the 1997 June spectra. Only one peak was present at some orbital phases (cf. Figures 9, 10 and 11). The velocity separation of the peaks ($\simeq 500 \text{ km s}^{-1}$) was larger than the radial velocity amplitude of the secondary star. This implies that the emission region was located within the orbit of the secondary star, thus ruling out the possibility of emission from the surface of the secondary (see also §4.3) or from a circumbinary disk.

According to Orosz & Bailyn (1997), the projected radial velocity semi-amplitude of the secondary star in GRO J1655–40 is $K_2 = 228.2 \pm 2.2 \text{ km s}^{-1}$, and the masses of the two components are $M_1 \simeq 7M_\odot$ and $M_2 \simeq 2.3M_\odot$. If we assume a thin, non-circular, Keplerian accretion disk truncated at the tidal radius, as described in Paczyński (1977), then the disk emission lines would have peaks with observed radial velocities at each phase given by the dash-dotted lines in Figure 13. The tidal truncation radius is approximately given by $R_d = 0.60a/(1+q)$ for $0.03 < q < 1$ (Warner 1995), where a is the separation between the centers of mass of the binary components. The peak-to-peak velocity separation averaged over an orbital cycle would be $\simeq 820 \text{ km s}^{-1}$. Phillips et al. (1999) derived lower values for the radial velocity semi-amplitude of the secondary star and for the masses of the binary components. They obtained $192 < K_2 < 214 \text{ km s}^{-1}$, $4.1 < M_1 < 6.6M_\odot$ and $1.4 < M_2 < 2.2M_\odot$ (90 per cent confidence limit). For a fixed mass ratio $q = 1/3$, this implies

that the peak-to-peak velocity separation averaged over an orbital cycle, expected from a tidally-truncated Keplerian disk, would be $690 < \Delta V < 760 \text{ km s}^{-1}$. Peak separations $\simeq 770 \text{ km s}^{-1}$ would instead be expected if we adopt the parameters determined by Shahbaz et al. (1999), who inferred a velocity semi-amplitude $K_2 = 215.5 \pm 2.4 \text{ km s}^{-1}$ for the companion star.

The velocity separations deduced from our 1996 June and 1997 June data are lower than the predicted values, especially for the red-shifted peak at phases around 0.5 and the blue-shifted peak at phases around 0. Therefore, the double-peaked profile of the $H\alpha$ emission component cannot be explained by a conventional thin Keplerian accretion disk truncated at the tidal radius. We note that the peak-to-peak velocity separations of He II $\lambda 4686$ and He I $\lambda 6678$ were also too small to be consistent with a tidally-truncated Keplerian disk.

Remarkably low rotational velocities, inconsistent with Keplerian disks truncated at their tidal radii, have also been inferred from the double-peaked $H\alpha$ emission line profiles observed from A0620–00 and GS 1124–68 (Orosz et al. 1994). A possible explanation for the low rotational velocities inferred for the outer edge of the accretion disks in these three systems is that the disks extended slightly beyond their tidal radii. (cf. Whitehurst 1988).

5.1.2. A schematic model

We have found that the observed variations in the $H\alpha$ line profile can be explained by the model shown in Figure 14, with two separate emission regions on the accretion disk. The model can reproduce the low radial velocities of the peaks and their behavior at various orbital phases. For example, only the red-shifted component would be visible around phase 0.5 and only the blue-shifted component around phase 1, while both peaks would be visible around phases 0.25 and 0.75.

Non-axisymmetric patterns of emission similar to our model were proposed by Steeghs, Harlaftis & Horne (1997) to explain the Balmer and helium emission line profiles observed from the dwarf nova IP Peg, and by Neustroev & Borisov (1998) to explain the Balmer line profiles observed from the dwarf nova U Gem. In both cases, they were interpreted as evidence of a two-armed spiral density wave or shock in the accretion disk, induced by the tidal interaction with the companion star. In the case of IP Peg, the observed rotational velocities also suggested that the disk could extend beyond its tidal radius (Steeghs et al. 1997).

It has been suggested that accretion stream overflows, hot spots, and uneven illumination of the accretion disk from the central X-ray source can also produce an anisotropic emissivity. However, it is beyond the scope of the present paper to explore in details why the Balmer emission regions might assume the geometrical configuration shown in our model.

Furthermore, a narrow $H\alpha$ absorption component from the companion star is also likely to be present, as suggested by the detection of other stellar absorption features from He I and Fe I. It

can be noticed from the radial velocity curve of the companion star that the presence of a stellar absorption line superimposed on the disk emission would also be qualitatively consistent with the observed behavior of the line profile at various orbital phases, if absorption and emission have comparable strength (Figures 9, 10 and 11). However, we argue that the effect of anisotropic disk emission is more significant than the effect of a stellar absorption line, and can better explain the velocity shifts of the emission peaks observed over an orbital phase.

One might expect the $H\alpha$ emission line profiles to be roughly symmetric at superior and inferior conjunction; however, the $H\alpha$ line in general showed a red-shifted peak stronger than the blue-shifted peak, and a blue wing more extended than the red wing (see Figure 9 and Figure 11). The asymmetry of the profiles may indicate the presence of both opacity and kinematic effects, and may be evidence of a thin disk-wind. It is worth noting that P-Cygni profiles were observed in some UV resonance lines from the system (Hynes et al. 1998b).

5.2. Formation of absorption and emission lines

5.2.1. Broad absorption lines

The $H\alpha$ and $H\beta$ lines in the spectra obtained during the 1996/1997 outburst all show broad (FWHM $\approx 3000 \text{ km s}^{-1}$), shallow absorption components. Broad absorption components are also seen in the 1994 August – September spectra, when the system was in outburst (see §6.2), but not in the 1996 April spectra, when the system was in quiescence.

Absorption lines can be produced in an accretion disk if the disk is optically thick and its temperature decreases with height above the central plane. The absorption features seen in our spectra are broader than the emission cores: this suggests that they were probably formed in the inner part of an optically thick disk, where viscous heating from the central plane dominates over external irradiative heating.

Broad, shallow absorption features at the Balmer lines have been seen in the spectra of other BHCs in outburst, such as A0620–00 (Whelan et al. 1977), GS 1124–68 (Della Valle, Masetti & Bianchini 1998) and, most prominently, GRO J0422+32 (Casares et al. 1995). Similar features are also often present in the spectra of UX UMa stars (e.g. Warner 1995) and in the outburst spectra of Dwarf Novae (Robinson, Marsh & Smak 1993).

5.2.2. Double-peaked emission lines

Double-peaked lines can be emitted from a hot temperature-inversion layer on the X-ray irradiated surface of the accretion disk. Provided that the spectrum is sufficiently soft, X-rays can be absorbed at a small depth, forming a thin temperature-inversion layer but leaving most of the ver-

tical structure of the disk undisturbed (see Tuchman, Mineshige & Wheeler 1990; Wu et al. 1999).

The strong, double-peaked He II $\lambda 4686$ line seen during the high-soft state in 1996–1997 was probably emitted via radiative recombination in this thin, hot layer, at temperatures $\sim 10^5$ K.

While the He II $\lambda 4686$ was detected throughout the 1996 outburst, Balmer emission was seen only after the hard X-rays turned on. Balmer lines are likely to be emitted at lower temperatures ($\sim 10^4$ K). Moreover, the H α double-peaked profile is strongly asymmetric and phase-dependent (§5.1.2), while the He II $\lambda 4686$ profile is approximately symmetric at *all* phases. For all these reasons we suggest that He II $\lambda 4686$ and the Balmer lines were emitted from different regions: the Balmer lines probably originated from a deeper, denser layer in the disk where matter was heated by harder X-ray photons.

6. ONSET OF A HARD X-RAY OUTBURST (1994 AUGUST – SEPTEMBER)

6.1. Overview

GRO J1655–40 was active in the radio and hard X-ray energy bands in 1994 August – September. The 843 MHz radio flux density, measured by the MOST, was declining after a large outburst that reached about 8 Jy in early August (Wu & Hunstead 1997). On 14 September another radio outburst started. It was weaker than the previous outburst, with a peak flux density of about 2 Jy.

The hard X-ray flux recorded by BATSE (Harmon et al. 1995) was below the 0.7 photon $\text{cm}^{-2} \text{s}^{-1}$ level during the period August 15 – September 4. A sharp rise in the X-ray flux occurred on September 5, and the flux stayed at the 2 photon $\text{cm}^{-2} \text{s}^{-1}$ level for about 10 days. It then declined abruptly, apparently in coincidence with the rise in the 843 MHz radio luminosity around September 14 (see Fig. 1 in Wu & Hunstead 1997).

The span of our observations covered the transition phase around the hard X-ray rapid increase. Good signal-to-noise spectra, with a resolution of 1.3 Å FWHM, in the spectral regions centered at H α and at He II/ H β , were obtained on August 30 – September 4, before the rise in the hard X-ray flux. The sampling of binary phase was roughly uniform over the six-night observations. Two lower-resolution spectra in the H α and He II/ H β regions were taken on 1994 September 6, after the rise in the X-ray flux, and showed a dramatic change compared with the August 30–September 4 spectra.

6.2. General spectral features before September 6

In Figure 15 we show the red spectrum, centered at H α , averaged over the six nights from August 30 to September 4. As in the spectra obtained during the 1996 – 1997 high-soft state, we notice a broad absorption component partly filled by narrow H α emission. The average EW of the

absorption component is $-6 \pm 1 \text{ \AA}$, and its average FWHM $60 \pm 10 \text{ \AA}$ ($\simeq 2700 \pm 500 \text{ km s}^{-1}$). The narrow emission component has an average EW = $5.3 \pm 0.2 \text{ \AA}$ and an average FWHM = $450 \pm 20 \text{ km s}^{-1}$.

Figure 16 shows the averaged blue spectrum, centered at He II/ H β . The broad absorption component of H β has an EW = $-4 \pm 1 \text{ \AA}$ and an FWHM = $50 \pm 10 \text{ \AA}$ ($\simeq 3000 \pm 600 \text{ km s}^{-1}$). A narrow emission component is superimposed on the broad absorption trough, with EW = $1.1 \pm 0.1 \text{ \AA}$ and FWHM = $550 \pm 30 \text{ km s}^{-1}$.

He II $\lambda 4686$ appears in the spectrum as a strong narrow emission line (Figure 16). The EW of the line is $5.2 \pm 0.2 \text{ \AA}$ and its FWHM is $540 \pm 20 \text{ km s}^{-1}$. Weaker emission is detected at He II $\lambda 4542$, with EW = $0.5 \pm 0.2 \text{ \AA}$ and FWHM = $800 \pm 50 \text{ km s}^{-1}$.

A broad emission component (FWHM = $950 \pm 100 \text{ km s}^{-1}$) was detected on each night at He I $\lambda 6678$. An additional narrower component (FWHM = $450 \pm 50 \text{ km s}^{-1}$) was detected on some nights; it was particularly strong on August 30 (cf. Figures 17). We note that this line might be contaminated by He II $\lambda 6683$ emission.

The spectra show a broad, flat-topped line at about 5005 \AA . It cannot be attributed to [O III] $\lambda 5007$ both because the wavelengths are discrepant, and because we do not see any emission from [O III] $\lambda 4959$, whose strength should be one-third of that of [O III] $\lambda 5007$. (The only forbidden lines possibly detected in our spectra obtained between 1994 August 30 and September 4 are [N II] $\lambda 6548$, blended with the much stronger blue wing of H α , and [N II] $\lambda 6589$; see Figures 17). We identify the line at about 5005 \AA as N II $\lambda 5005$.

Another strong low-ionization metal line detected in the spectrum is the blend O II $\lambda\lambda 4941, 4943$. Other broad emission lines detected from N II and O II are listed in Table 3. We do not include a weak emission line at 6375 \AA in Table 3, as it was seen only on the first two nights (EW = 0.7 ± 0.1); its wavelength is consistent with that of an Fe X line. Bowen N III emission lines were also observed, broader than in 1996 June, and with a radial velocity curve consistent with that of the primary rather than the secondary.

6.3. Line classification

The FWHMs of the optical lines observed before 1994 September 6 span a large range of values, from $\lesssim 400 \text{ km s}^{-1}$ to $\approx 3000 \text{ km s}^{-1}$. The broadest lines are those seen in absorption at H α and H β . We notice that a broad absorption trough at H β was also detected in the 1995 March outburst by Bianchini et al. (1997), and during the 1996 May–June high-soft state. The physical interpretation of the broad Balmer absorption lines is probably the same as discussed in §5.2.1. Henceforth, we will focus only on the emission lines.

For the orbital parameters of GRO J1655–40, the projected rotational velocity of the outer rim of a thin, Keplerian accretion disk, truncated at or slightly beyond its tidal radius, is $\gtrsim 350$

km s⁻¹. Therefore, any lines with an FWHM < 700 km s⁻¹ cannot come from a thin Keplerian disk. We classify the emission lines observed before 1994 September 6 as “broad” and “narrow” (Table 3), according to whether their FWHM was larger or smaller than the minimum value of FWHM expected for disk emission.

The broad emission lines were usually flat-topped, while the narrow emission lines were either single-peaked or had a hint of a double-peaked profile but with very low velocity separation. In some cases the distinction is blurred, especially for the weak lines. However, in most situations the two kinds of line profiles can be discerned. We notice that both the EW and the FWHM of the narrow lines changed significantly from night to night, while EW and FWHM of the broad lines were more stable.

Our phenomenological classification of broad and narrow emission lines in GRO J1655–40 is similar to the classification of emission lines in AGNs. For example, a study of 123 high-luminosity AGNs (Wills et al. 1993) has shown that the profile of the C IV λ 1549 emission line consists of a “broad” base and a “narrow” core, which are emitted from distinct regions. The FWHM of the line is determined by the core/base ratio: when the core is dominant, the line will appear narrow and sharply peaked; and when the base is dominant the line will be broad and flat-topped (cf. Fig. 2 in Wills et al. 1993).

6.3.1. Origin of the “broad” emission lines

The low-ionization metal lines from N II and O II detected in our spectra are examples of broad emission lines; their FWHMs are consistent with a disk origin. Unlike the disk emission lines seen in 1996 June, their profiles were generally flat-topped rather than double-peaked.

Flat-topped lines can be emitted in a wind from the surface of the accretion disk. Murray & Chiang (1997) showed that if the lines have substantial optical depth ($\tau_l \gtrsim 1$), the contribution of the wind from the front and back sectors of the disk (where the projected radial velocities are lower) is enhanced relative to the contribution of the wind from the sides of the disk (where the projected radial velocities are higher), thus smearing out the two peaks in the line profile.

From the fact that we detected only low-ionization broad lines from He I, O II, N II and N III, we infer an ionization parameter $U \equiv L_x/n_H r^2 \approx 10$ in the line-emitting disk wind. The corresponding temperature would be $\sim 1 - 2 \times 10^4$ K if the gas was collisionally ionized (Hatchett, Buff & McCray 1976); the temperature would be lower if the line-emitting gas was photoionized.

The possibility of an outflow or disk wind suggested by the broad optical emission line profiles observed in the 1994 X-ray outburst was already discussed in Hunstead et al. (1997), who compared the spectrum of GRO J1655–40 with the spectra of WN6-8 Wolf-Rayet stars. In spite of the similarities, there are several differences between the two cases. Firstly, high-ionization emission lines usually found in WR stars, e.g. from N IV and N V, were not observed, indicating a lower

temperature for the outflow in GRO J1655–40. Secondly, no forbidden [O III] lines were observed, implying a higher density. Thirdly, the broad, flat-topped profiles are better explained by a disk-wind model rather than by a spherical outflow as in typical Wolf-Rayet stars.

6.3.2. Kinematics of the “narrow” emission lines

The narrow emission lines showed large night-to-night changes in their EWs and line profiles. In particular, they showed transitions between narrow, single-peaked and slightly broader, double-peaked profiles over the time-span of our observations. We notice that He II $\lambda 4686$ line was generally broader and more clearly double-peaked than H α (Figure 18; cf. also the double-peaked profile in the combined spectrum shown in Figure 16); its peak-to-peak velocity separation was however always $< 400 \text{ km s}^{-1}$.

Some lines (most notably He I $\lambda 6678$) were probably emitted from both the broad- and the narrow-line regions, with the intensity ratio determined by the relative contribution of the two components, i.e. as in the “base” vs “core” classification scheme suggested by Wills et al. (1993) in their study of AGNs.

Both the H α and He II $\lambda 4686$ emission lines were, on average, asymmetric; they were slightly blue-shifted with respect to the central line wavelength (taking into account the systemic velocity). In the combined spectrum of all six nights, the H α line is blue-shifted by $55 \pm 9 \text{ km s}^{-1}$, the H β line by $61 \pm 12 \text{ km s}^{-1}$, the narrow component of the He I $\lambda 6678$ line by $82 \pm 22 \text{ km s}^{-1}$, and the He II $\lambda 4686$ line by $41 \pm 13 \text{ km s}^{-1}$. We note that a similar phenomenon is often observed in the emission lines from quasars and in some cataclysmic variables, and can be attributed to the expansion of clouds or to a gas outflow, when the receding gas is occulted from our view.

6.3.3. Optically thin narrow-emission-line region

Owing to the well-determined orbital parameters, the upper limit to the size of the accretion disk in GRO J1655–40 is reasonably well constrained. We have found that the velocities inferred from the narrow widths of the H α , H β and He II $\lambda 4686$ lines were significantly lower than the velocities expected from a Keplerian disk contained in the Roche lobe of the compact star.

One might argue that the low FWHM of the narrow emission lines was due to their formation in a circumbinary disk (Artymowicz & Lubow 1996). If this were true, no significant velocity shifts from the center-of-mass systemic velocity should be seen over an orbital cycle. However, Soria et al. (1998) have measured the radial velocity shifts of the line wings at one-quarter of the maximum intensity above the continuum, and found a sinusoidal variation consistent with the one observed in 1996 June, which was interpreted as the modulation due to orbital motion of the compact star. Moreover, the profiles of these lines changed substantially from night to night. In

the case of $H\alpha$, the line profile was single-peaked on four nights, but double-peaked on the other two, with a velocity separation larger than expected from a circumbinary disk. We can therefore rule out the possibility of emission from a circumbinary disk.

We interpret the narrow lines, instead, as emission from a spheroidal or extended optically thin region high above the accretion disk (at lower rotational velocity). We notice that some cataclysmic variables show narrow, often single-peaked Balmer and He II emission lines, yielding rotational velocities much slower than Keplerian. For example, there is strong evidence of an optically thin line-emitting region extended well above the disk plane in the eclipsing system PG 1012–029 (Honeycutt, Schlegel & Kaitchuck 1986). The larger FWHM of the high-ionization He II line suggests that it was probably emitted closer to the disk plane than $H\alpha$, and/or at slightly smaller radii, where we expect the irradiation from the central source to be stronger.

The night-to-night variability in the line profiles (Figure 18) might reflect changes in the line-of-sight opacity of the optically thin region. Opacity variations can be caused by matter inhomogeneities (i.e. moving clouds) in the line emission region or variable obscuration along the light path. Furthermore, the variability between single-peaked and double-peaked profiles indicates that the extended line-emitting region was not in steady state; for instance, the profiles would tend to become broader and more “disk-like” (as those observed in 1996 June) as the thin clouds dissipated, and less “disk-like” when the emission from the clouds was stronger.

The presence of optically thin line-emitting gas well above the disk plane may be explained in various ways: some accreting matter might not yet have settled down onto the disk, after the end of the strong hard X-ray flare observed by BATSE in 1994 August. We shall argue in §6.4.2 that the outer disk is likely to be disrupted and puffed up into a thick torus during a hard X-ray flare. Some of the gas in the extended narrow-line region may also have been the result of bipolar outflows from the disk surface, as suggested by the systematic blue-shift and by the detection of strong winds in the broad-line region.

The extended, optically thin narrow-line-region model is valid only if the UV and soft X-ray flux is not too high. Soft irradiating flux of order of the Eddington limit at distances $R < 10^{12}$ cm would yield an ionization parameter $U > 10^4$ in the thin narrow-line region, for a gas with densities $n_H < 10^{13}$ cm $^{-3}$. This would imply temperatures $\gtrsim 10^7$ K, difficult to reconcile with the presence of lines such as $H\alpha$. Although no UV and soft X-ray data were obtained at that epoch, the fact that we detected only low-ionization metal lines (for example from N II and O II) implies that the soft flux could not have been too strong in the 1994 X-ray outburst.

6.4. Spectral transition on 1994 September 6

6.4.1. General features

A sharp increase in the hard X-ray flux was detected by BATSE around September 5 (Harmon et al. 1995). The broad N II, N III and O II emission lines disappeared from the blue spectrum obtained on September 6 (Figure 19), and He II $\lambda 4686$ and the Bowen N III lines were much weaker than in the previous nights. $H\alpha$ and $H\beta$ were instead much stronger: for $H\alpha$, $EW = 100 \pm 5 \text{ \AA}$, and for $H\beta$, $EW = 8.0 \pm 0.5 \text{ \AA}$. The low-resolution of the red spectrum does not allow for a reliable determination of the FWHM of $H\alpha$; for $H\beta$, $FWHM = 530 \pm 50 \text{ km s}^{-1}$. The $H\alpha/H\beta$ EW ratio increased by a factor of 4 between September 4 and September 6. Other lines clearly seen in emission are the Paschen series of H I and several He I lines ($\lambda 4922$, $\lambda 5016$, $\lambda 5876$, $\lambda 6678$, $\lambda 7065$). All these emission lines were single-peaked; unfortunately, the low S/N of the blue spectrum and the low resolution of the red spectrum do not permit an accurate determination of their strengths and widths.

The sudden increase in the Balmer emission between September 4 and September 6 coincided with the sharp increase in the hard X-ray flux. The EWs (in absolute value) of $H\alpha$, $H\beta$ and He II $\lambda 4686$ are shown in Figure 20 compared with the hard X-ray flux measured by BATSE. The Balmer EWs and the hard X-ray flux appear well correlated, as in the 1996 June observations. Such correlation is not seen for He II $\lambda 4686$. In fact, its intensity dropped when the the hard X-ray flux rose.

Shrader et al. (1996) also noticed the dramatic increase in the $H\alpha$ emission and the disappearance of He II $\lambda 4686$ around TJD 9600, after the hard X-ray flux surge (see their Fig. 1). Their low-resolution spectrum obtained on September 8 showed only emission from the low-ionization lines H I, He I and O I.

Optical spectra taken by Bianchini et al. (1997) on 1994, August 12 – 15, during the decline of an earlier hard X-ray flare, showed emission almost as strong as that in our September 6 spectrum from low-ionization lines like $H\alpha$ (mean $EW = 68.4 \text{ \AA}$) and $H\beta$ (mean $EW = 7.4 \text{ \AA}$). The $H\alpha/H\beta$ EW ratio was 9.2, a factor of 3 higher than on September 4, and slightly lower than on September 6. The high-ionization He II $\lambda 4686$ (mean $EW = 5.3 \text{ \AA}$) and N III $\lambda\lambda 4641, 4642$ (mean $EW = 5.9 \text{ \AA}$) lines were also present, showing disk or disk-wind signatures (see Fig. 2 in Bianchini et al. 1997). From the peak separation and the width of the flat-topped profiles, we can infer that the outer-disk radius was $\lesssim (1.3 \pm 0.1) \times 10^{11} \text{ cm}$. Broad absorption troughs were not seen in those spectra.

We suspect that the conditions on August 12 – 15 were intermediate between those we observed before and after September 5. In the period of low X-ray activity between August 15 and September 5, a geometrically thin accretion disk was probably re-forming and re-expanding to its tidal radius after having been disrupted in the previous hard X-ray flare, only to be then “evaporated” again into an extended atmosphere or cocoon by the following flare.

6.4.2. *Optically thick Balmer emission*

As the photoionization cross-section for hydrogenic ions falls approximately as $\nu^{-7/2}$ for photon energies larger than the threshold energy (13.6 eV for hydrogen) (see Osterbrock 1989), the hard (20 – 100 keV) X-ray photons contribute little to the ionization level of the gas, compared with the UV and soft X-ray photons. However, Compton heating by the hard X-rays can alter the disk structure and drive a disk-wind (e.g. Begelman, McKee & Shields 1983; Idan & Shaviv 1996). In the extreme conditions, the dense disk-wind would create a cocoon surrounding the accretion disk; in this situation one may consider the accretion disk being practically evaporated into a thick atmosphere. The absence of the characteristic broad absorption troughs at $H\alpha$ and $H\beta$ and of broad disk-like emission lines in our September 6 spectrum suggests the absence of an exposed, geometrically thin, optically thick accretion disk.

An increase in the optical depth of the corona could have caused the increase in Balmer line emission and the disappearance of the high-ionization lines. The higher $H\alpha/H\beta$ EW ratio measured during the 1994 August and September hard X-ray flares, and the Paschen emission lines observed on September 6, indicate that the corona was optically thick in the Balmer series. When this situation occurs, every $H\beta$ photon is resonantly absorbed by a nearby hydrogen atom in the $n = 2$ state; the process of emission and reabsorption is repeated until the $H\beta$ photon splits into $H\alpha + P\alpha$ photons, which will both escape (“Case C” recombination, see e.g. McCray 1996).

After the end of the 1994 August hard X-ray flare, the extended cocoon probably became optically thin to the Balmer lines (“Case B” recombination), as observed on August 30 – September 4. The disk was “puffed up” again by the hard X-ray flare after September 4, so that Balmer lines were emitted via Case C recombination. Archival spectra obtained from the Anglo-Australian Observatory, taken on September 27 (Figure 21), show features almost identical to those observed on August 30 – September 4 (cf. Figures 15 and 16), suggesting that the cocoon once again became optically thin after the end of the second hard X-ray flare.

The simultaneous decrease in the observed strength of the He II and Bowen N III lines at the time of the hard X-ray increase can perhaps be attributed to a geometric effects. As GRO J1655–40 has a high orbital inclination, a thick outer-disk rim, inflated by hard X-ray irradiation, may occult the inner region where the high-ionization lines are formed, and explain their weakness in the September 6 spectrum.

Finally, we note that a major episode of plasma ejection occurred on 1994 September 9, inferred from the radio observations (Harmon et al. 1995; see also Wu & Hunstead 1997), a few days after the change in the optical and hard X-ray spectra. It was suggested (Fabian & Rees 1995) that there may be a connection between the production of collimated jets and the presence of an extended hot, high pressure atmosphere and a quasi-spherical accretion flow in the centers of elliptical galaxies, the usual hosts for radio-loud emission. Whether the same mechanism was a catalyst for the collimated ejections observed in the radio-loud outburst of GRO J1655–40 in 1994 August – September is an issue worth investigating.

7. SUMMARY

We have obtained optical spectra of the soft X-ray transient GRO J1655–40 during different energy states (quiescence, high-soft and hard outburst) between 1994 August and 1997 June.

Spectra taken one day after the observed brightening in V in 1996 April did not at that stage show evidence of emission lines from an accretion disk. The main spectral features were narrow absorption lines from the secondary star. The optical brightening was probably due to an increase in the continuum emission from the disk; emission lines could not be formed at that stage, in the absence of X-ray irradiation.

For the 1996 – 97 high-soft state, we have identified characteristic features such as broad absorption lines at $H\alpha$ and $H\beta$, partly filled by double-peaked emission lines. We argue that the broad absorption was formed in the hot inner disk, and the double-peaked He II $\lambda 4686$ emission originated in a temperature-inversion layer on the disk surface, created by the soft X-ray irradiation. The observed rotational velocities suggest that the disk was probably extended beyond its tidal radius. We have also found that the double-peaked $H\alpha$ emission was associated with the hard X-ray flux, suggesting that it was probably emitted at comparable radii but from deeper layers (at higher optical depth) than He II $\lambda 4686$. We note that the Balmer lines were not emitted uniformly from the whole disk surface, but appeared to come only from a double-armed region, possibly the effect of tidal density waves or shocks on the disk.

We have identified three classes of lines in the spectra taken in 1994 August – September before the onset of a hard X-ray flare: broad absorption, broad (flat-topped) emission and narrow emission. The narrow emission line profiles cannot be explained by a conventional thin accretion disk model. We speculate that the system was in a transient state in which the accretion disk had an extended, optically thin cocoon and significant matter outflow, which would also help to explain the systematic blue-shift of the narrow emission lines and the flat-topped profiles of the broad emission lines.

After the onset of a hard X-ray flare, the disk signatures disappeared, and strong $H\alpha$ and Paschen emission was detected, suggesting that the cocoon became optically thick to the Balmer lines. High-ionization lines disappeared or weakened. Two weeks after the end of the flare, the cocoon appeared to be once again optically thin.

We thank: David Buckley, Gary Da Costa, Paul Francis, Charlene Heisler and Raffaella Morganti for taking some of the spectra; Alan Harmon and Shuang-Nan Zhang for the BATSE data and discussions; and Geoff Bicknell, Ralph Sutherland, Martijn de Kool, Stefan Wagner and John Greenhill for comments and discussions. R. W. H. acknowledges financial assistance from the Australian Research Council, and thanks his co-observers in 1994 August – September, Max Pettini, Dave King and Linda Smith, for their tolerance in allowing the ToO observations to displace some of the scheduled observing program. K. W. acknowledges support from the ARC through an Australian Research Fellowship and the support from S. N. Zhang for the visits to NASA-MSFC and

UAH.

REFERENCES

- Artymowicz, P., & Lubow, S. H. 1996, *ApJ*, 467, L77
- Bailyn, C. D., et al. 1995a, *Nature*, 374, 701
- Bailyn, C. D., Orosz, J. A., McClintock, J. E., & Remillard, R. A. 1995b, *Nature*, 378, 157
- Begelman, M. C., McKee, C. F., & Shields, G. A. 1983, *ApJ*, 271, 70
- Bianchini, A., Della Valle, M., Masetti, N., & Margoni, R. 1997, *A&A*, 321, 477
- Casares, J., Marsh, T. R., Charles, P. A., Martin, A. C., Martín, E. L., Harlaftis, E. T., Pavlenko, E. P., & Wagner, R. M. 1995, *MNRAS*, 274, 565
- Della Valle, M., Masetti, N., & Bianchini, A. 1998, *A&A*, 329, 606
- Edelson, R. A., & Krolik, J. H. 1988, *ApJ*, 333, 646
- Fabian, A. C., & Rees, M. J. 1995, *MNRAS*, 277, L55
- Harmon, B. A., et al. 1995, *Nature*, 374, 703
- Hatchett, S., Buff, J., & McCray, R. 1976, *ApJ*, 206, 847
- Hjellming, R. M. 1997, in *Accretion Phenomena and Related Outflows*, IAU Colloquium 163, eds D. T. Wickramasinghe, G. V. Bicknell & L. Ferrario, ASP Conference Series, 121, 53
- Hjellming, R. M., & Rupen, M. P. 1995, *Nature*, 375, 464
- Honeycutt, R. K., Schlegel, E. M., & Kaitchuck R. H. 1986, *ApJ*, 302, 388
- Horne, K., & Marsh, T. R. 1986, *MNRAS*, 218, 761
- Horne, K., et al. 1996, *IAU Circ.* 6406
- Hunstead, R. W., & Campbell-Wilson, D. 1996, *IAU Circ.* 6410
- Hunstead, R. W., Wu, K., & Campbell-Wilson, D. 1997, in *Accretion Phenomena and Related Outflows*, IAU Colloquium 163, eds D. T. Wickramasinghe, G. V. Bicknell & L. Ferrario, ASP Conference Series, 121, 63
- Hynes, R.I., Haswell, C. A., Shrader, C. R., Chen, W., Horne, K., Harlaftis, E. T., O'Brien, K., Hellier, C., & Fender, R. P. 1998b, *MNRAS*, 300, 64
- Hynes, R.I., O'Brien, K., Horne, K., Chen, W., & Haswell, C. A. 1998a, *MNRAS*, 299, 37
- Idan, I., & Shaviv, G. 1996, *MNRAS*, 281, 615
- Kumar, S. 1986, *MNRAS*, 223, 225
- Levine, A. M., Bradt, H., Cui, W., Jernigan, J. G., Morgan, E. H., Remillard, R. A., Shirey, R. E., & Smith, D. A. 1996, *ApJ*, 469, L33
- McClintock, J. E. 1998, in *Accretion Processes in Astrophysical Systems: Some Like it Hot*, eds S. S. Holt & T. R. Kallman, AIP Conference Proceedings, 431, 290

- McCray, R. 1996, in IAU Colloquium 145, Supernovae and Supernova Remnants, ed. R. McCray & Z.-R. Wang (Cambridge: Cambridge University Press), 223
- Murray, N., & Chiang, J. 1997, *ApJ*, 474, 91
- Neustroev, V. V., & Borisov, N. V. 1998, *A&A*, 336, L73
- Orosz, J. A., Bailyn, C. D., Remillard, R. A., McClintock, J. E., & Foltz, C. B. 1994, *ApJ*, 436, 848
- Orosz, J. A., Remillard, R. A., Bailyn, C. D., & McClintock, J. E. 1997, *ApJ*, 478, L83
- Orosz, J. A., & Bailyn, C. D. 1997, *ApJ*, 477, 876. See also Erratum: Orosz, J. A., & Bailyn, C. D. 1997, *ApJ*, 482, 1086
- Osterbrock, D. E. 1989, *Astrophysics of Gaseous Nebulae and Active Galactic Nuclei* (Mill Valley: University Science Books)
- Paczyński, B. 1977, *ApJ*, 216, 822
- Phillips, S. N., Shahbaz, T., & Podsiadlowsky, Ph. 1999, *MNRAS*, 304, 839
- Remillard, R. A., Bradt, H., Cui, W., Levine, A. M., Morgan, E. H., Shirey, R. E., & Smith, D. A. 1996, *IAU Circ.* 6393
- Robinson, E. L., Marsh, T. R., & Smak, J. I. 1993, in *Accretion Disks in Compact Stellar Systems*, ed. J. C. Wheeler (Singapore: World Scientific), 75
- Shahbaz, T., van der Hooft, F., Casares, J., Charles, P. A., & van Paradijs, J. 1999, *MNRAS*, 306, 89
- Shrader, C. R., Wagner, R. M., Hjellming, R. M., & Starrfield, S. G. 1996, *A&AS*, 120, 261
- Smak, J. I. 1981, *Acta Astron.*, 31, 395
- Soria, R., Wickramasinghe, D. T., Hunstead, R. W., & Wu, K. 1998, *ApJ*, 495, L95
- Steenhals, D., Harlaftis, E. T., & Horne, K. 1997, *MNRAS*, 290, L28
- Tanaka, Y., & Lewin W. H. G. 1995, in *X-Ray Binaries*, eds W. H. G. Lewin, J. van Paradijs, & E. P. J. van den Heuvel (Cambridge: Cambridge University Press), 126
- Tavani, M., Fruchter, A., Zhang, S.-N., Harmon, B. A., Hjellming, R. N., Rupen, M. P., Bailyn, C., & Livio, M. 1996, *ApJ*, 473, L103
- Tingay, S. J. et al. 1995, *Nature*, 374, 141
- Tuchman, Y., Mineshige, S., & Wheeler, J. C. 1990, *ApJ*, 359, 164
- van der Hooft, F., Heemskerk, M. H. M., Alberts, F., & van Paradijs, J. 1998, *A&A*, 329, 538
- Warner, B. 1995, in *Cataclysmic Variable Stars* (Cambridge: Cambridge University Press)
- Whelan, J. A. J., Ward, M. J., Allen, D. A., Danziger, I. J., Fosbury, R. A. E., Murdin, P. G., Penston, M. W., Peterson, B. A., Wampler, E. J., & Webster, B. L. 1977, *MNRAS*, 180, 657
- Whitehurst, R. 1988, *MNRAS*, 232, 35

- Wills, B. J., Brotherton, M. S., Fang, D., Steidel, C. C., & Sargent, W. L. W. 1993, *ApJ*, 415, 563
- Wu, K., & Hunstead, R. W. 1997, in *Accretion Phenomena and Related Outflows*, IAU Colloquium 163, eds D. T. Wickramasinghe, G. V. Bicknell & L. Ferrario, ASP Conference Series, 121, 835
- Wu, K., Soria, R., Hunstead, R. W., & Johnston, H. 1999, *MNRAS* submitted
- Zhang, S. N., et al. 1994, *IAU Circ.* 6046

Table 1. Physical parameters for GRO J1655–40

		Ref.
Distance	$d = 3.2 \pm 0.2$ kpc	a
	$3 < d < 5$ kpc	b
Binary period	$P = 2.62157 \pm 0.00015$ d	c
	$P = 2.62168(14)$ d	d
Inclination angle	$i = 69^\circ.5 \pm 0^\circ.08$	c
	$63^\circ.7 < i < 70^\circ.7$	d
Mass ratio	$q = 0.334 \pm 0.009$	c
	$0.337 < q < 0.436$	e
Mass function	$f_X = 3.24 \pm 0.09 M_\odot$	c
	$f_X = 2.73 \pm 0.09 M_\odot$	e
	$1.93 < f_X < 2.67 M_\odot$	f
Mass of primary	$M_1 = 7.02 \pm 0.22 M_\odot$	c
	$5.5 < M_1 < 7.9 M_\odot$	e
	$4.1 < M_1 < 6.6 M_\odot$	f
Mass of secondary	$M_2 = 2.34 \pm 0.12 M_\odot$	c
	$1.7 < M_2 < 3.3 M_\odot$	e
	$1.4 < M_2 < 2.2 M_\odot$	f
Systemic velocity	$\gamma = -142.4 \pm 1.6$ km s ⁻¹	c
	$\gamma = -141.9 \pm 1.3$ km s ⁻¹	e
	$-153 < \gamma < -143$ km s ⁻¹	f
Quiescent V mag	17.3	g

^aHjellming & Rupen 1995

^bTingay et al. 1995

^cOrosz & Bailyn 1997

^dvan der Hooft et al. 1998

^eShahbaz et al. 1999

^fPhillips et al. 1999

^gBailyn et al. 1995

Table 2. Our spectroscopic observations of GRO J1655–40

Date	Epoch (HJD - 2449000)	Phase range	Wavelength range (Å)	Resolution (Å FWHM)
AAT 3.9 m				
1994 August 26	590.969–590.976	0.359–0.362	5645–7240	3.5
1994 August 29	593.947–593.954	0.495–0.498	3780–7450	7.3
1994 August 30	594.866–594.883	0.846–0.852	6280–6825	1.3
	594.897–594.909	0.858–0.862	4432–5051	1.3
1994 August 31	595.863–595.877	0.226–0.231	6280–6825	1.3
	595.885–595.899	0.234–0.240	4432–5051	1.3
1994 September 1	596.867–596.883	0.609–0.615	6280–6825	1.3
	596.888–596.911	0.617–0.626	4432–5051	1.3
1994 September 2	597.857–597.870	0.987–0.992	6280–6825	1.3
	597.872–597.885	0.992–0.997	4432–5051	1.3
1994 September 3	598.860–598.873	0.369–0.374	6280–6825	1.3
	598.875–598.894	0.375–0.382	4432–5051	1.3
1994 September 4	599.860–599.873	0.751–0.756	6280–6825	1.3
	599.882–599.895	0.759–0.764	4432–5051	1.3
1994 September 6	601.861–601.864	0.514–0.515	5500–11000	20
			3925–5500	2.5
ANU 2.3 m				
1996 April 20	1194.259–1194.303	0.485–0.501	3600–9300	4.8
1996 April 21	1195.096–1195.151	0.804–0.824	3600–9300	4.8
1996 June 8	1242.980–1243.327	0.069–0.202	4360–5320	1.3
			6300–7250	1.3
1996 June 9	1243.893–1244.285	0.418–0.567	4150–5115	1.3
			6300–7250	1.3
1996 June 10	1244.868–1245.292	0.790–0.951	4150–5115	1.3
			6300–7250	1.3
1996 June 11	1245.885–1246.153	0.178–0.280	4150–5115	1.3
			6300–7250	1.3
1996 June 12	1246.877–1247.293	0.556–0.715	4150–5115	1.3
			6300–7250	1.3
1996 June 17	1252.029–1252.052	0.521–0.530	6300–7250	1.3
1997 June 14	1614.010–1614.092	0.599–0.630	4150–5115	1.3
			6300–7250	1.3
1997 June 15	1615.056–1615.243	0.998–0.069	4150–5115	1.3
			6300–7250	1.3

Table 3. Main permitted lines detected during the 1994 outburst

Line	EW (\AA)	FWHM (km s^{-1})
BROAD ABSORPTION LINES		
H β λ 4861	-4 ± 1	3000 ± 600
H α λ 6562	-6 ± 1	2700 ± 500
BROAD EMISSION LINES		
O II λ 4452	0.7 ± 0.2	1350 ± 150
N III λ 4515	0.7 ± 0.2	950 ± 50
He II λ 4542	0.5 ± 0.2	800 ± 50
O II $\lambda\lambda\lambda$ 4602, 4609, 4613 ^a	2.1 ± 0.2	1400 ± 150
N III $\lambda\lambda$ 4641, 4642 ^b	5.0 ± 0.5	1050 ± 100
O II $\lambda\lambda$ 4941, 4943 ^c	1.9 ± 0.1	1750 ± 50
N II λ 5005	1.0 ± 0.1	1400 ± 50
He I λ 6678 ^{d,e}	0.9 ± 0.1	950 ± 100
NARROW EMISSION LINES		
H α λ 6562	5.3 ± 0.2	450 ± 20
H β λ 4861	1.1 ± 0.1	550 ± 30
He II λ 4686	5.2 ± 0.2	540 ± 20
He I λ 6678 ^{e,f}	0.9 ± 0.1	380 ± 40

^aPossible contribution also from N II $\lambda\lambda\lambda$ 4601, 4607, 4614 and (less likely) from N IV λ 4606.

^bafter deblending a small contribution from N II λ 4631; possible contribution also from N III λ 4634.

^cafter deblending a small contribution from He I λ 4922.

^d“broad” component of the line.

^ePossible contribution also from He II λ 6683.

^f“narrow” component of the line.

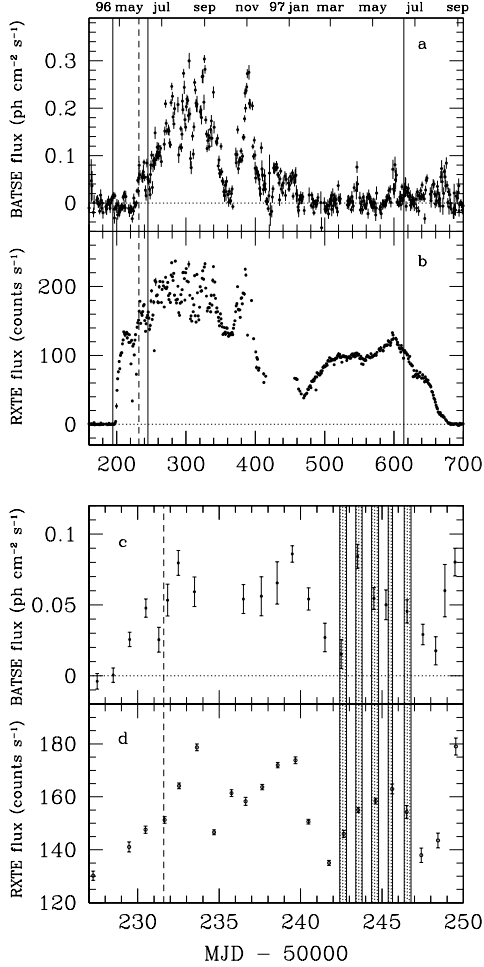


Fig. 1.— a: daily averages of the hard (20 – 100 keV) X-ray flux measured by BATSE. b: daily averages of the soft (2 – 12 keV) X-ray flux measured by RXTE/ASM. The lightcurves cover the period from 1996 March 18 to 1997 September 9. The solid lines mark the epochs of our observations (1996 April 20–21, 1996 June 8–12, 1997 June 14–15). A transition from quiescence to a high-soft X-ray spectral state occurred around MJD 50198 (April 25). The X-ray spectrum hardened after MJD 50230 (May 27). A radio flare was observed by MOST on MJD 50232 (May 28.60 UT) (dashed line). Hjellming (1997) estimates that the peak of the radio flare occurred sometime between MJD 50222.5 and MJD 50230.5. The actual onset of the radio flare is not well determined: its flux density was already declining with an e-folding time of 1.4 d when the flare was detected (Hunstead et al. 1997). In the lower panels, we show an expanded view of the hard (c) and soft (d) X-ray flux around the time of our 1996 June observations (shaded regions).

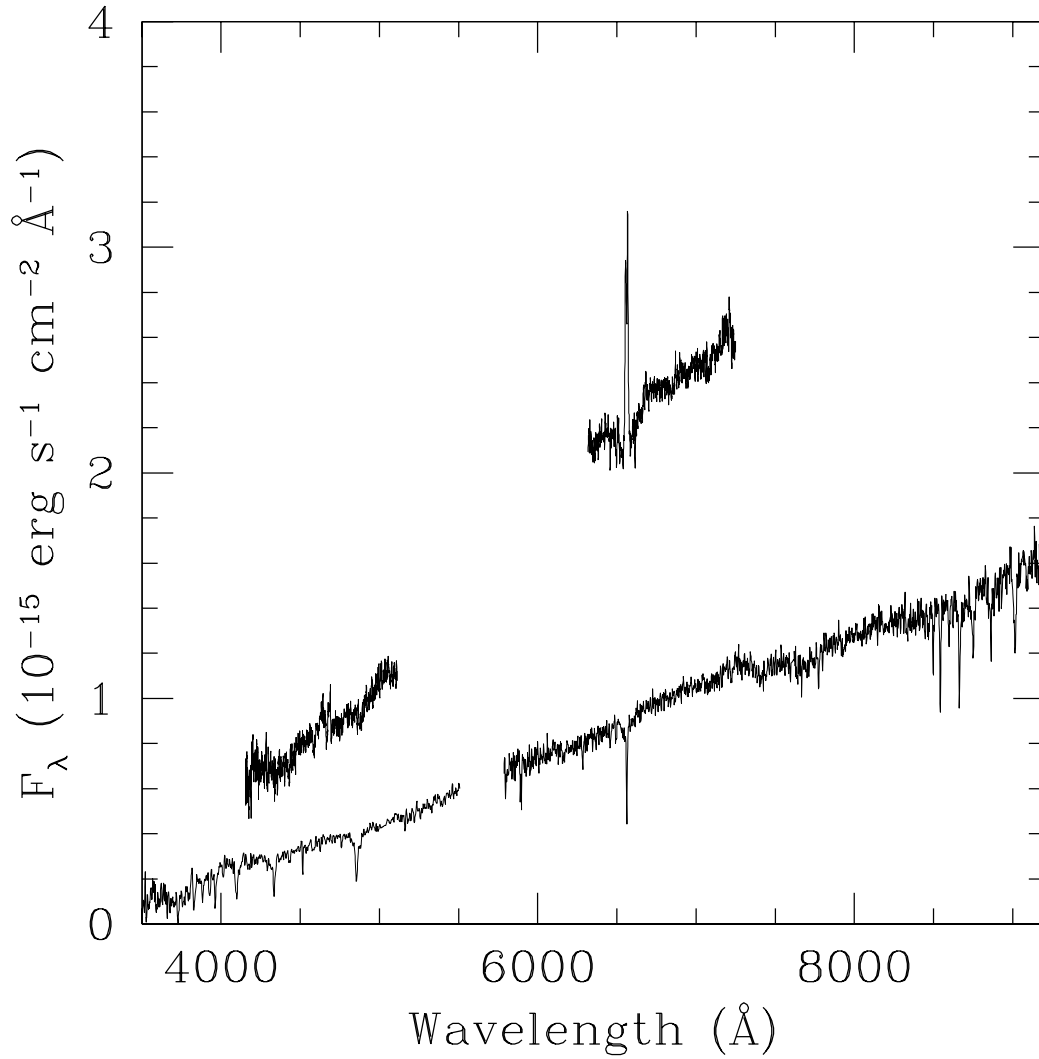


Fig. 2.— Flux-calibrated spectra taken on 1996 April 21 (lower spectrum) and on 1996 June 10 (upper spectrum) with the ANU 2.3 m telescope at Siding Spring Observatory. Wavelengths are vacuum heliocentric (cf. Figure 2 in Hynes et al. 1998b).

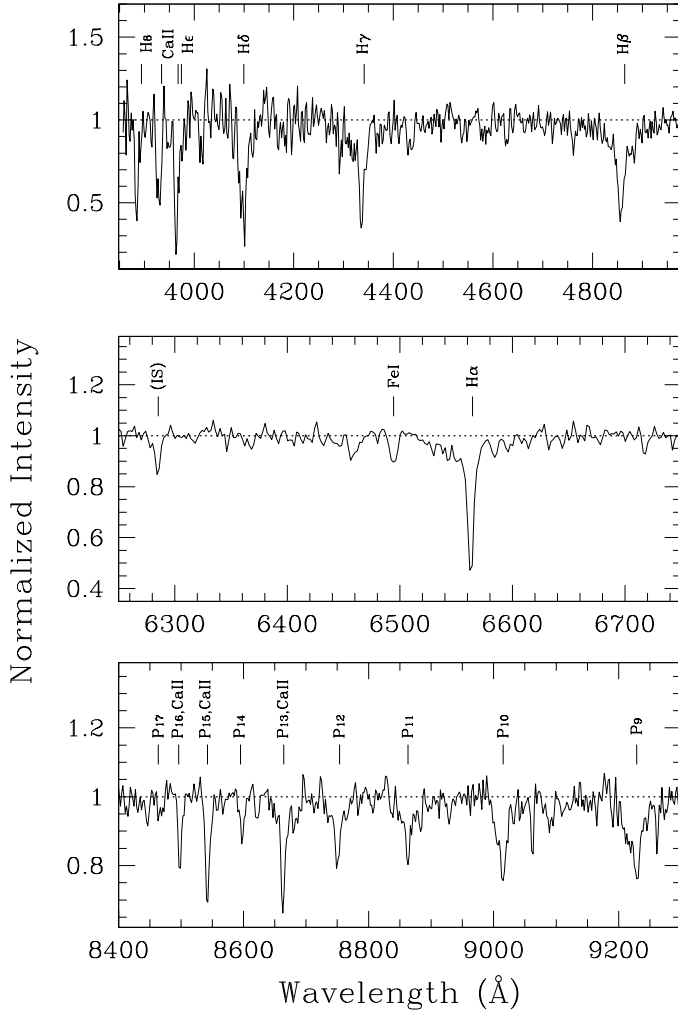


Fig. 3.— Top panel: averaged blue spectrum obtained on 1996 April 20, at spectroscopic phases $0.485 < \phi < 0.501$, according to the ephemeris of Orosz & Bailyn (1997). Central and bottom panels: portions of the averaged red spectrum obtained on 1996 April 21, at spectroscopic phases $0.804 < \phi < 0.824$. Wavelengths are vacuum heliocentric, and the intensities are normalized to the continuum. The Balmer series is in absorption. Other strong absorption features are H I Paschen series, Ca II $\lambda\lambda 3934, 3968$ (the latter is blended with He $\lambda 3970$), and the triplet Ca II $\lambda\lambda 8542, 8662, 8498$ (blended with the Paschen lines). No emission is observed from the N III/C III lines, nor from He II $\lambda 4686$.

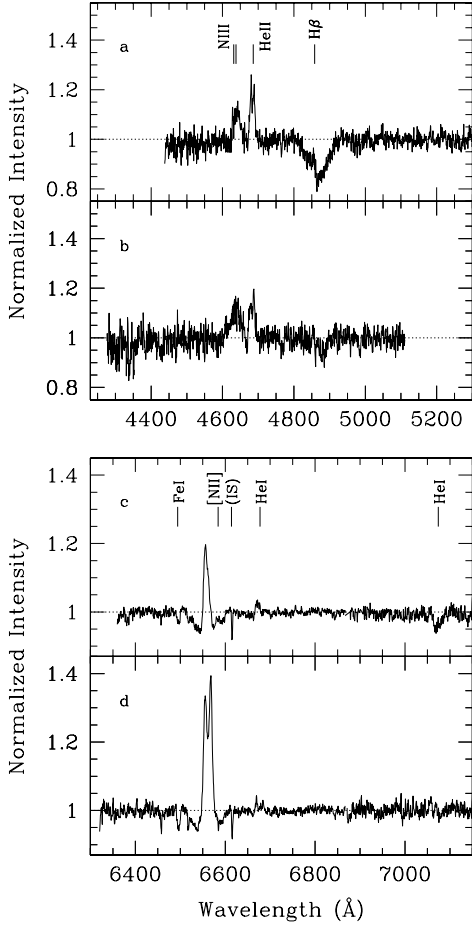


Fig. 4.— a: normalized blue spectrum taken on 1996 June 8, around spectroscopic phase $\phi = 0.10$. b: normalized blue spectrum taken on 1996 June 10, around $\phi = 0.85$. c: normalized red spectrum taken on 1996 June 8, around $\phi = 0.10$. d: normalized red spectrum taken on 1996 June 10, around $\phi = 0.85$. Wavelengths are vacuum heliocentric. Broad absorption troughs were detected at $H\beta$ and $H\alpha$ on June 8; they were partly filled on June 10. A broad absorption feature at He I $\lambda 7065$ was also present in the June 8 spectrum, but had disappeared on June 10. Emission was observed from the Bowen fluorescence lines of N III (single-peaked) and from He II $\lambda 4686$, $H\alpha$ and He I $\lambda 6678$ (double-peaked). The $H\alpha$ emission was much stronger on June 10 than on June 8. The peak-to-peak separations for He II $\lambda 4686$ lines were $525 \pm 25 \text{ km s}^{-1}$ on June 8, and $545 \pm 25 \text{ km s}^{-1}$ on June 10. The peak-to-peak separation for $H\alpha$ was $550 \pm 10 \text{ km s}^{-1}$ on June 10; on the same night, the peak-to-peak separation for He I $\lambda 6678$ was $650 \pm 50 \text{ km s}^{-1}$.

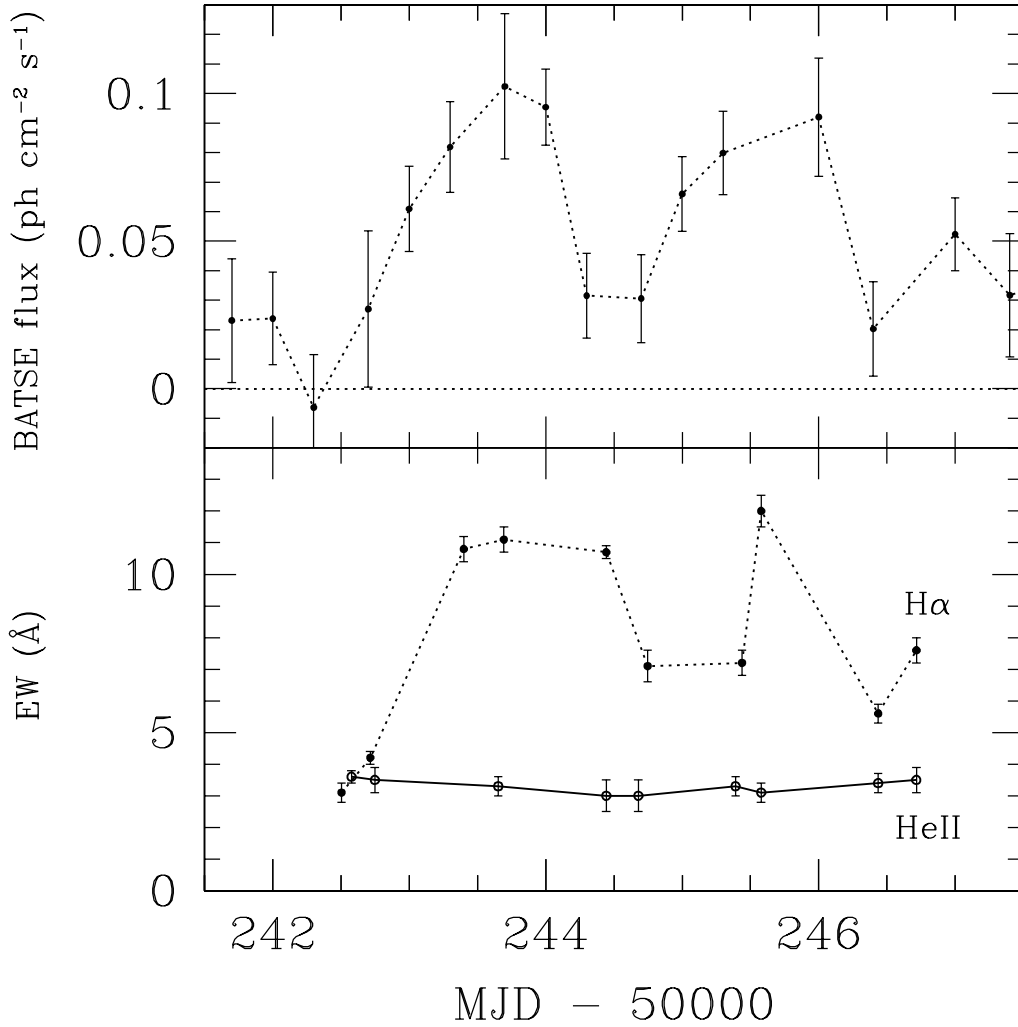


Fig. 5.— Top panel: hard (20 – 100 keV) X-ray flux measured by BATSE during the time of our 1996 June observations. Bottom panel: equivalent width of the H α and He II λ 4686 emission lines. No correlation was found between the hard X-ray flux and the EW of He II λ 4686, but there is evidence of a correlation between the hard X-ray flux and the H α emission. A similar correlation was observed in 1994 August – September (cf. Figure 20).

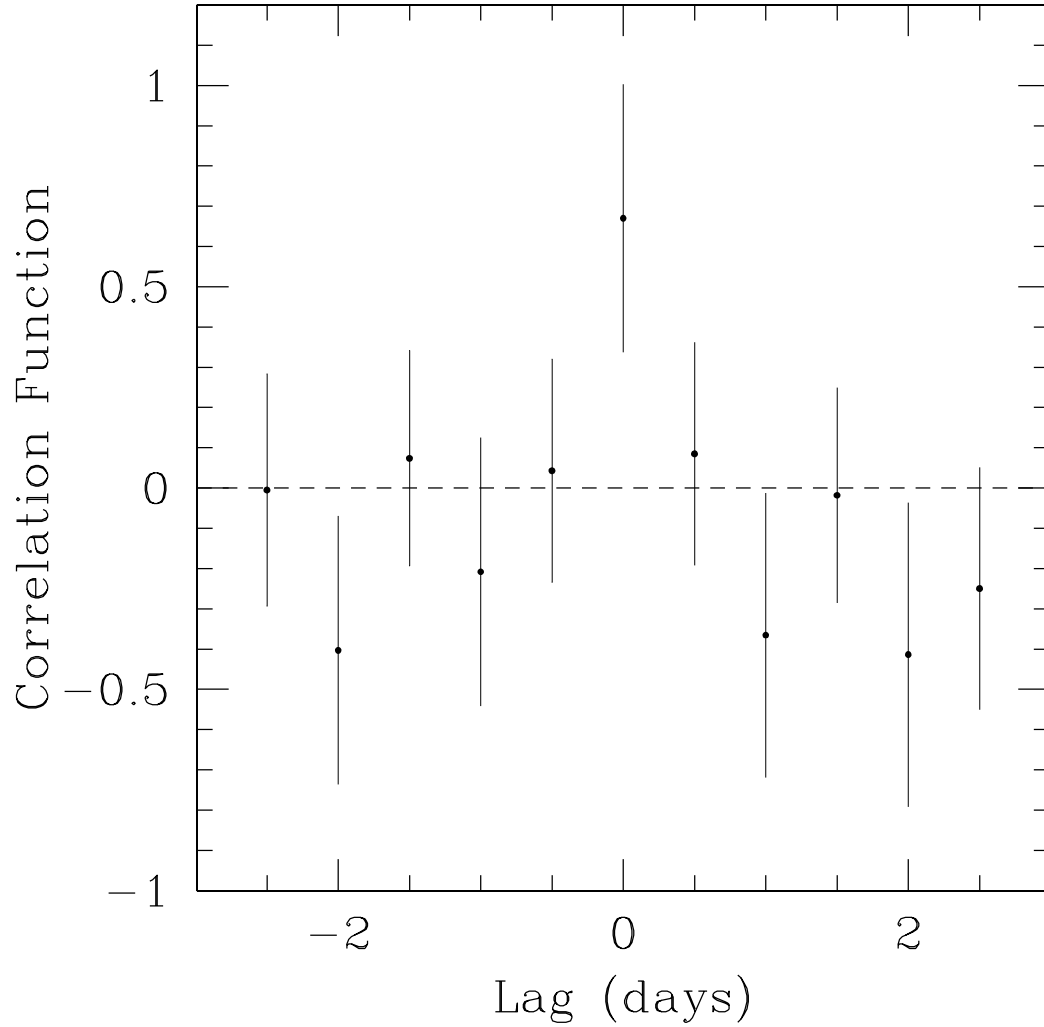


Fig. 6.— Discrete cross-correlation function for the equivalent width of the $H\alpha$ emission line and the hard (20 – 100 keV) X-ray flux in 1996 June. The error is large, mainly because of the limited number of datapoints available for the correlation function; nonetheless, the two quantities appear correlated. Better evidence of a correlation between hard X-ray flux and Balmer emission was found in our 1994 observations (cf. Figure 20).

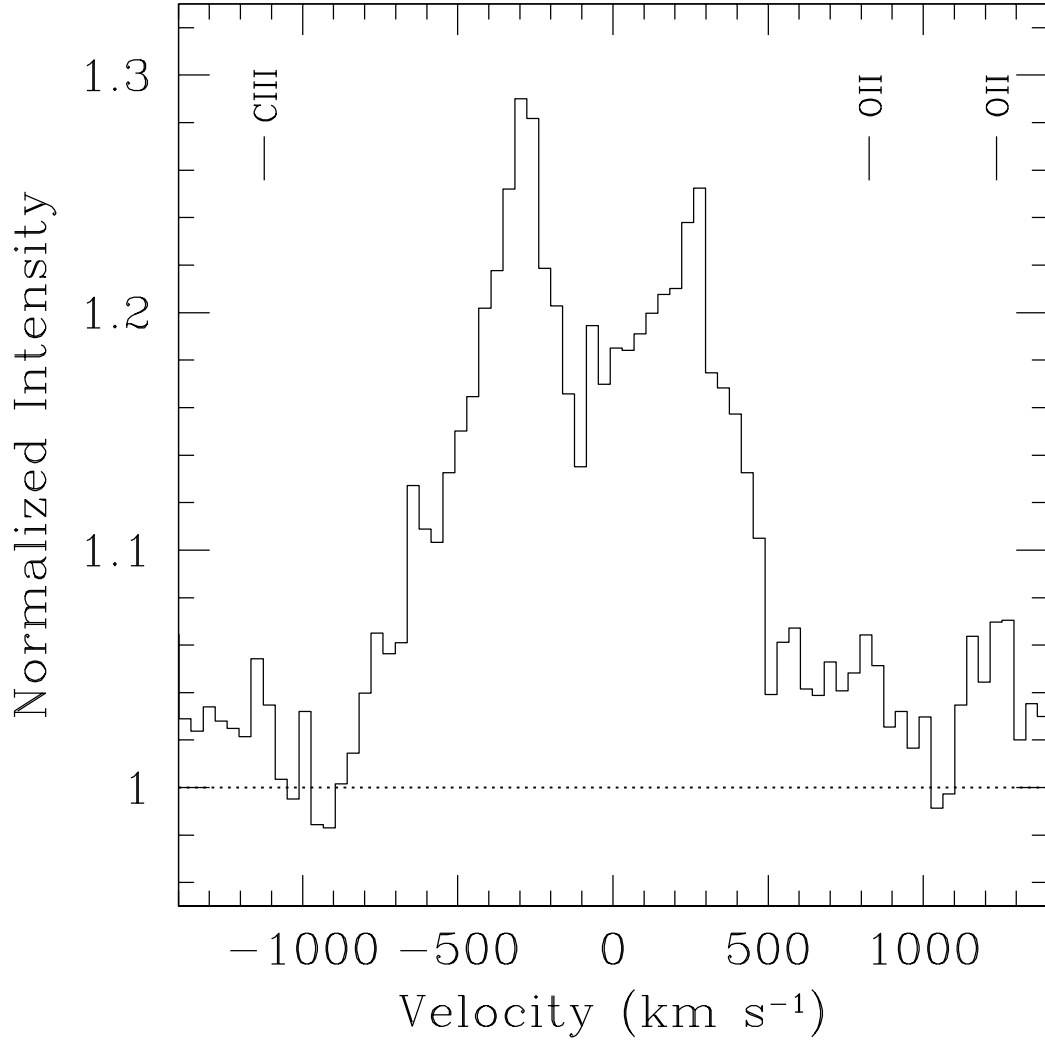


Fig. 7.— Normalized line profile of He II $\lambda 4686$, obtained by averaging the spectra taken on 1996 June 8 at orbital phases $0.08 < \phi < 0.12$. Wavelengths are vacuum heliocentric and the intensity is normalized to the continuum. The velocity zeropoint is the systemic velocity ($\gamma = -142.4 \pm 1.6$ km s⁻¹, see Table 1). Weak emission is also detected at positions consistent with C III $\lambda 4664$, O II $\lambda 4699$ and O II $\lambda 4705$, as marked in the figure.

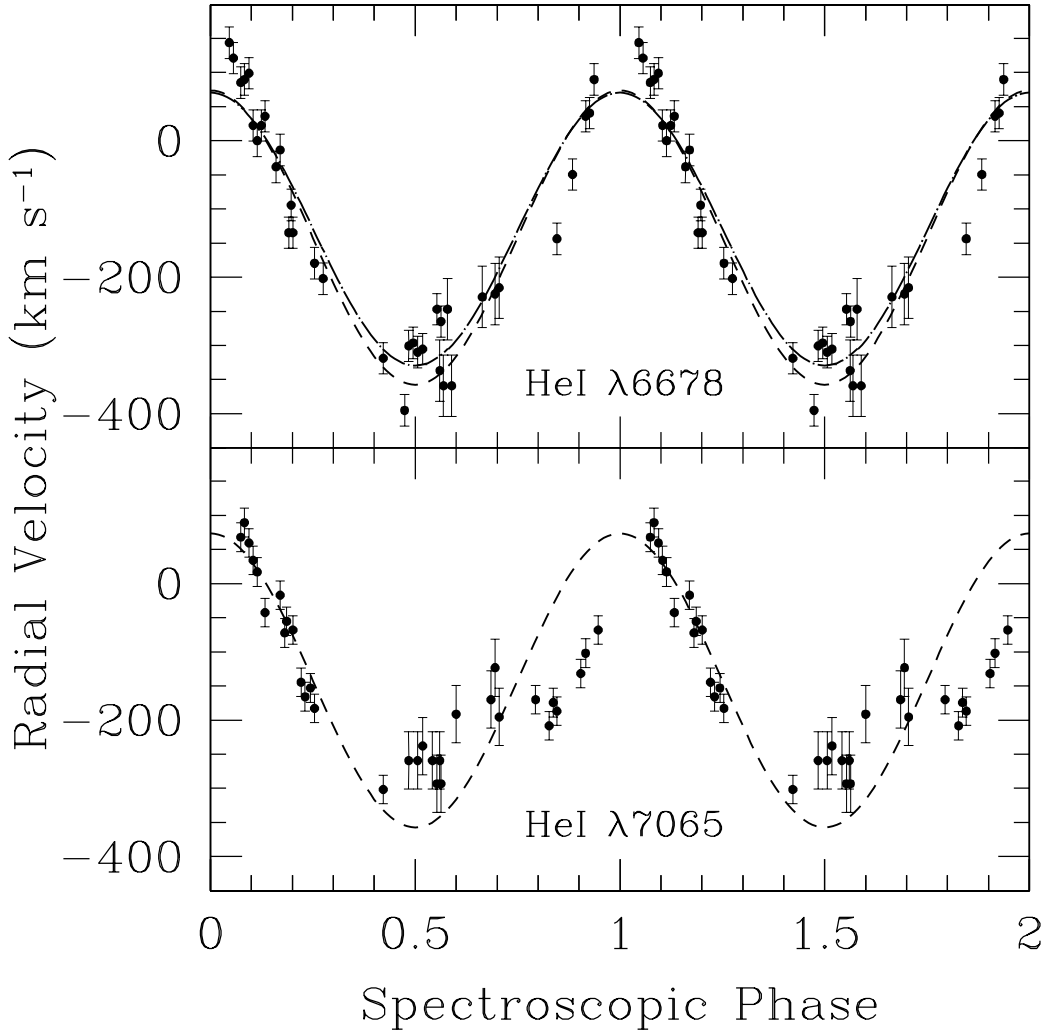


Fig. 8.— Radial velocity shifts of the narrow absorption components observed at He I $\lambda 6678$ (top panel) and He I $\lambda 7065$ (bottom panel) in 1996 June. Dash-dotted line (top panel): best sinusoidal fit to the velocity shifts of He I $\lambda 6678$ (semi-amplitude $K = 199.9 \pm 6.4$ km s⁻¹). Dashed line: projected radial velocity of the secondary star according to Shahbaz et al. (1999) (semi-amplitude $K = 215.5 \pm 2.4$ km s⁻¹).

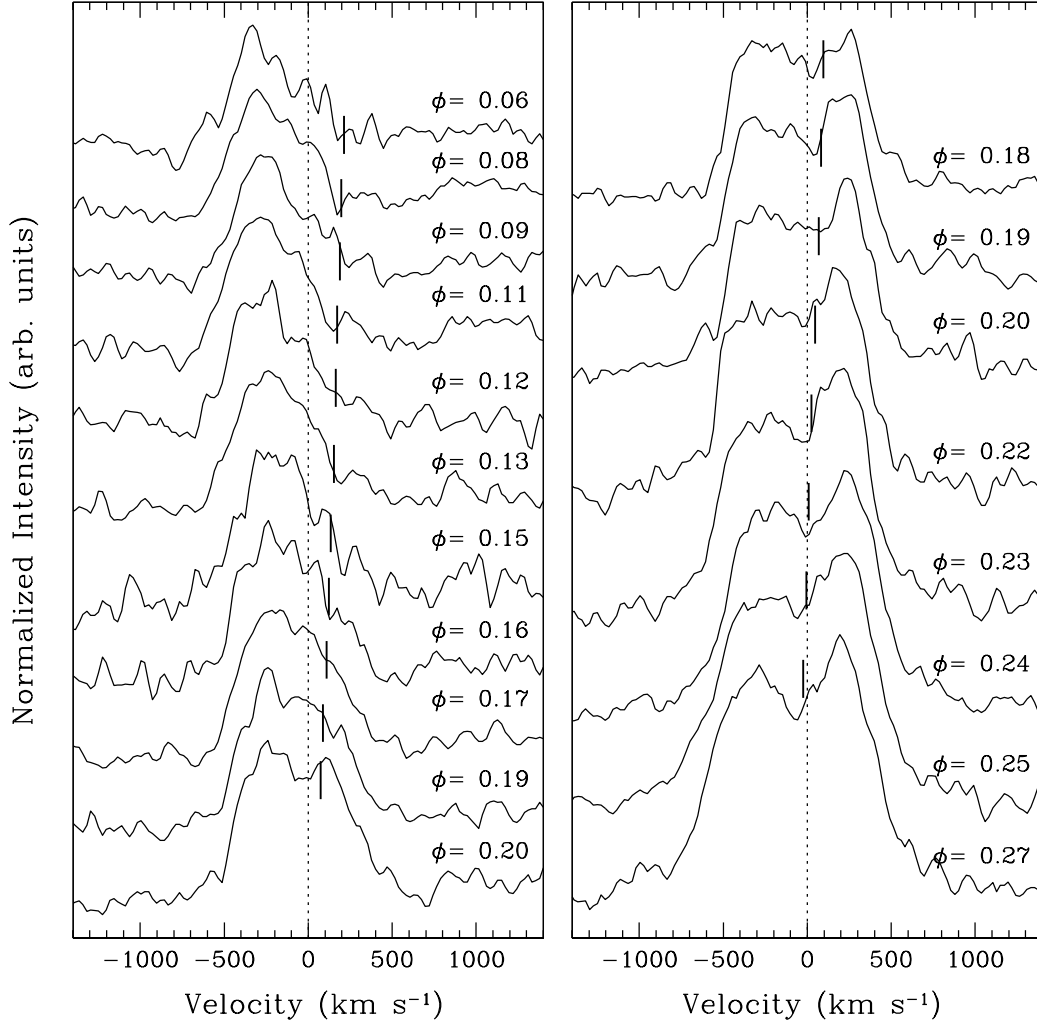


Fig. 9.— $H\alpha$ emission line profiles observed on 1996 June 8 (left panel) at spectroscopic phases $0.06 < \phi < 0.20$, and on June 11 (right panel), at phases $0.18 < \phi < 0.27$. The velocity zeropoint (dotted line) is the systemic velocity ($\gamma = -142.4 \pm 1.6 \text{ km s}^{-1}$). The projected radial velocities of the secondary star with respect to the systemic velocity are also shown next to each spectrum (short solid lines). Note that when the secondary star was receding from us, the largest contribution to the $H\alpha$ emission was coming from approaching gas. Both the red and the blue peak were visible when the secondary star was near superior conjunction.

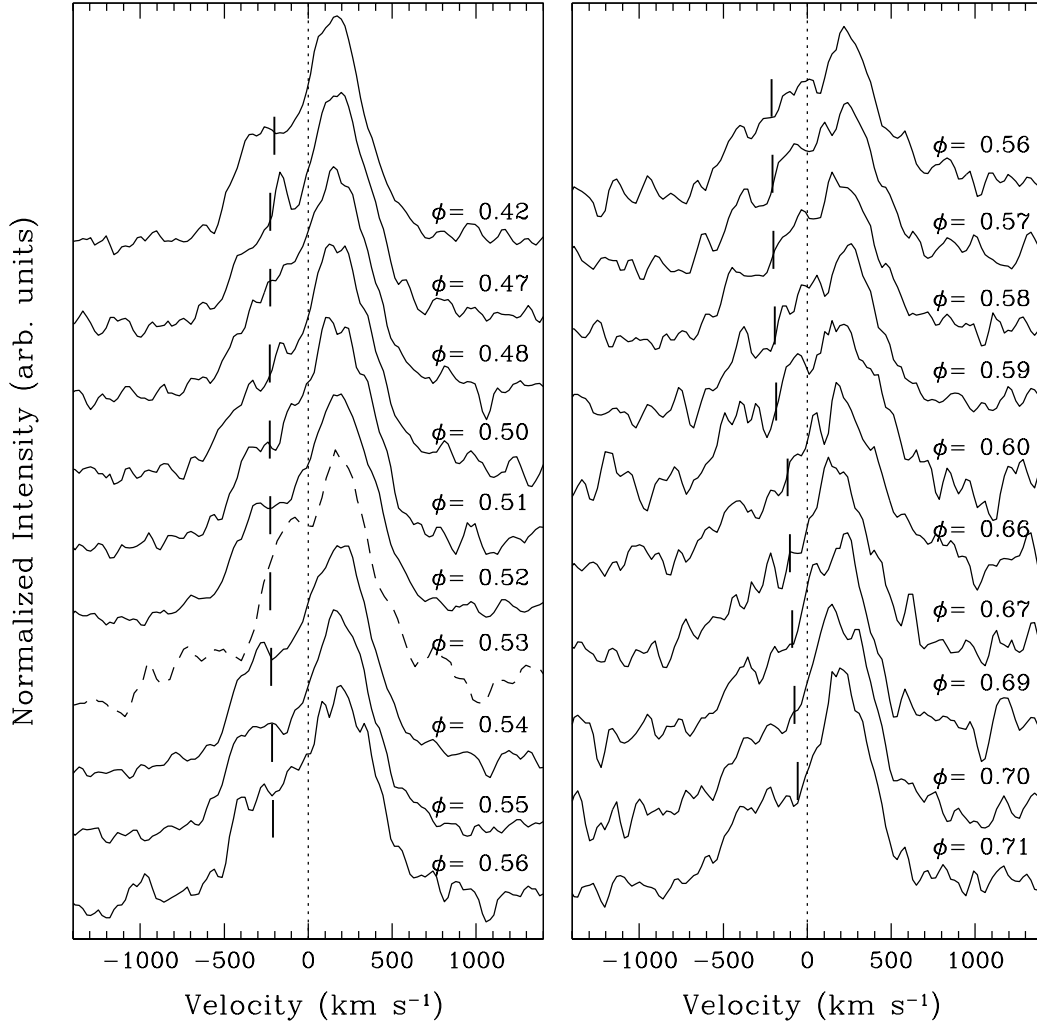


Fig. 10.— As in Fig. 9, for the 1996 June 9 observations (left panel), at spectroscopic phases $0.42 < \phi < 0.56$, and the June 12 observations (right panel), at phases $0.56 < \phi < 0.71$. The dashed profile in the left panel was obtained on 1996 June 17. Note that while the secondary star was approaching us, most of the emission was coming from receding gas. A narrow absorption feature, with a velocity consistent with the velocity of the companion star, is visible for $0.5 \lesssim \phi \lesssim 0.7$, superimposed on the emission profile.

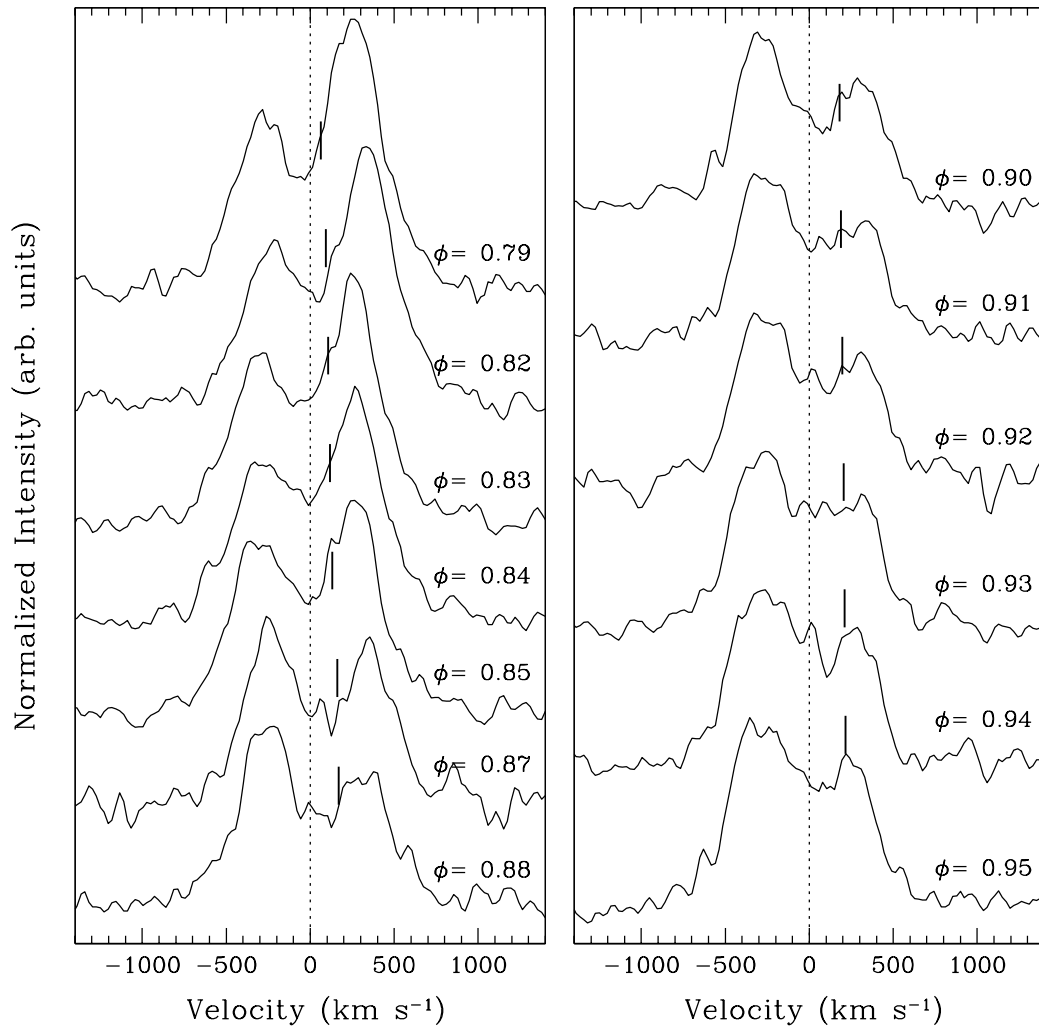


Fig. 11.— As in Fig. 9, for the 1996 June 10 observations, at spectroscopic phases $0.79 < \phi < 0.88$ (left panel) and at phases $0.90 < \phi < 0.95$ (right panel).

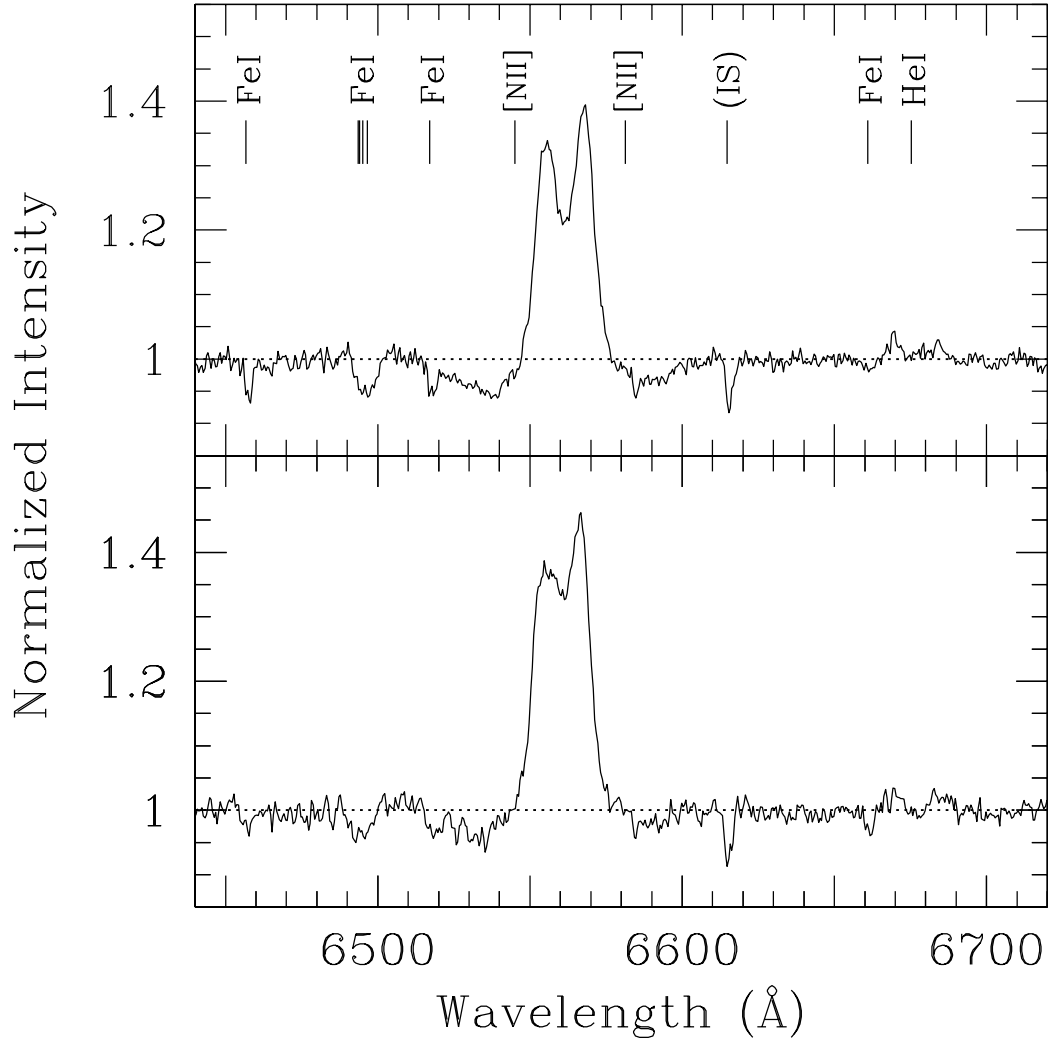


Fig. 12.— Top panel: normalized averaged spectrum in the $H\alpha$ region, obtained on 1996 June 10, at spectroscopic phases $0.80 < \phi < 0.92$. Bottom panel: normalized averaged spectrum obtained on 1996 June 11, at phases $0.19 < \phi < 0.28$. Wavelengths are vacuum heliocentric. Double-peaked emission was observed at $H\alpha$ and He I $\lambda 6678$. Weak [N II] $\lambda 6548$ and [N II] $\lambda 6584$ emission lines were probably blended with the wings of $H\alpha$. Narrow Fe I absorption lines, probably from the secondary star, were also seen. (They appear broadened here because the spectra have been averaged over a large phase interval; in particular, they appear double-peaked in the top panel because the spectra at $\phi \simeq 0.80$ and $\phi \simeq 0.90$ give the largest contribution to the average spectrum.)

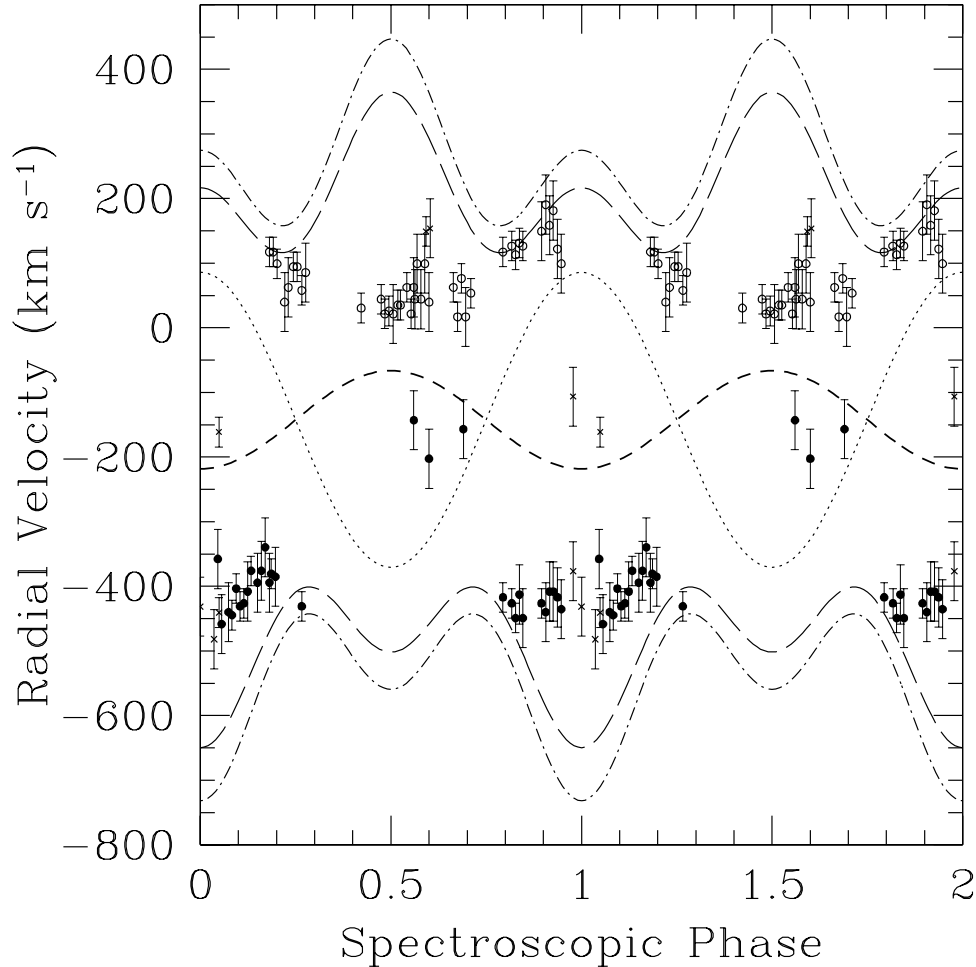


Fig. 13.— Velocities of the peaks detected in the H α emission line profiles, as a function of spectroscopic binary phase, compared with other characteristic velocities of the system. The zeropoint in the velocity scale is referred to the heliocentric system; the systemic velocity of the centre of mass is taken as $-142.4 \pm 1.6 \text{ km s}^{-1}$ (Table 1). Open and filled circles indicate the velocity shifts of the red and blue peaks respectively, detected in the 1996 June spectra. Crosses indicate the peaks detected in the 1997 June spectra. The short-dashed line is the projected radial velocity of the primary star, and the dotted line is the projected radial velocity of the secondary star, as determined by Orosz & Bailyn (1997). (Smaller velocities for the two components were inferred by Phillips et al. 1999 and Shahbaz et al. 1999). The dash-dotted lines are the projected velocities of the two edges of a non-circular Keplerian disk truncated at the tidal radius, as calculated by Paczyński (1977), for the system parameters determined by Orosz & Bailyn (1997); the long-dashed lines are calculated for the system parameters determined by Phillips et al. (1999). The velocity corresponding to the parameters inferred by Shahbaz et al. 1999 would be intermediate between the two.

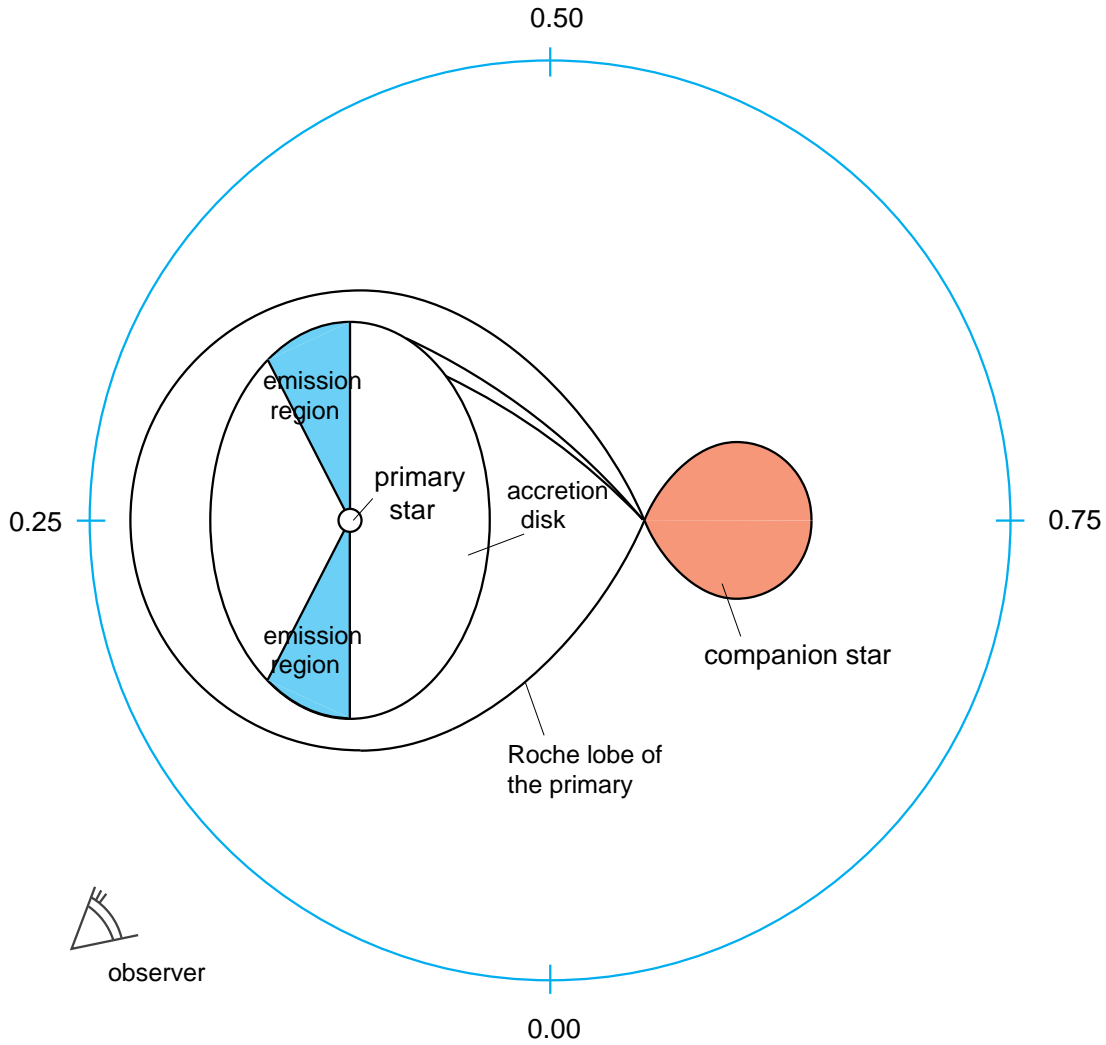


Fig. 14.— Schematic elliptical disk model that can reproduce the low velocity separations of the $H\alpha$ emission-line peaks, and the line profile variations over an orbital period as observed in 1996 June and 1997 June. In the model, $H\alpha$ would be emitted mostly from the shaded regions. We do see both emitting regions at all phases, but it can be noticed from the figure that at some phases both regions are blue-shifted (around phase 0) or red-shifted (around phase 0.5).

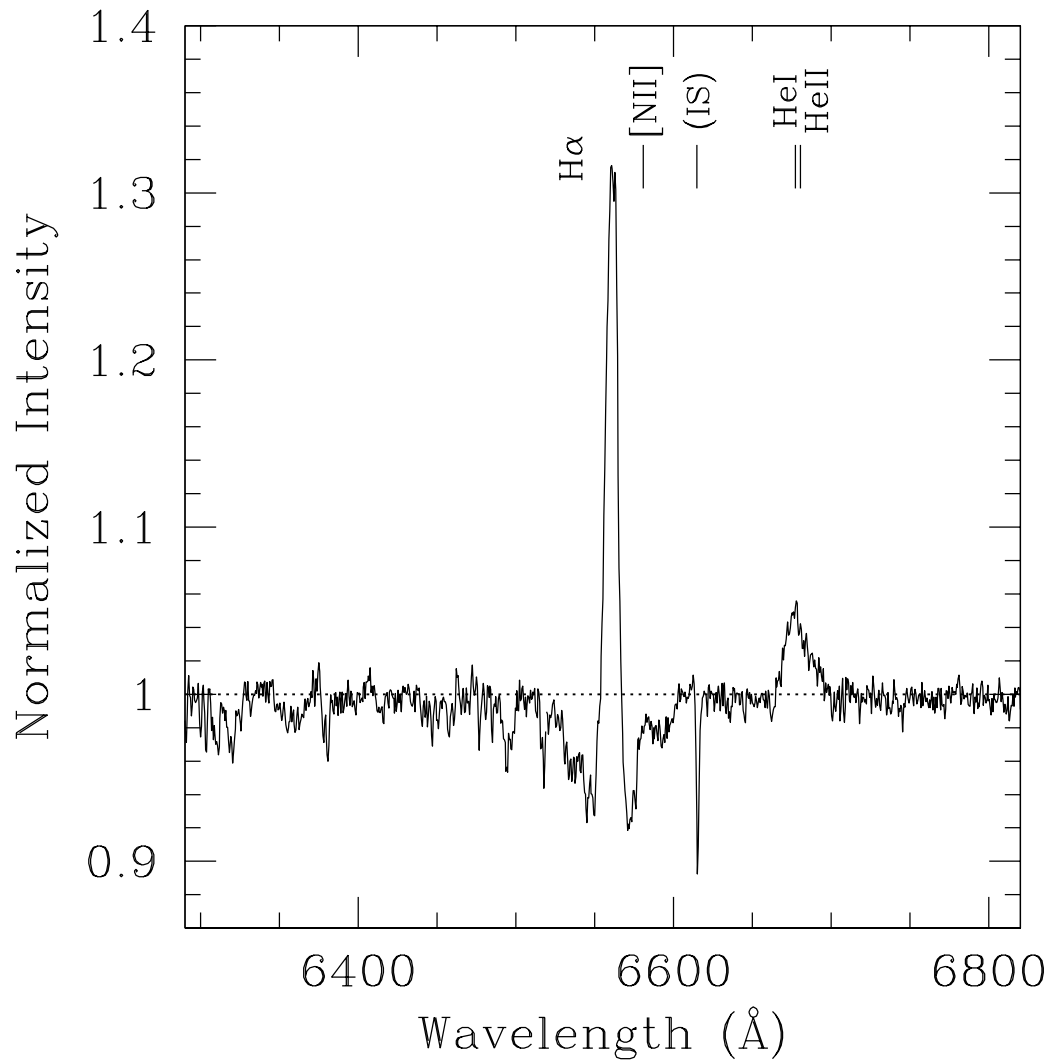


Fig. 15.— Averaged red spectrum obtained by combining the spectra taken from 1994 August 30 to September 4 with the 3.9 m Anglo-Australian Telescope at Siding Spring Observatory. Wavelengths are vacuum heliocentric and the intensity is normalized to the continuum. The most prominent features in the spectrum are marked.

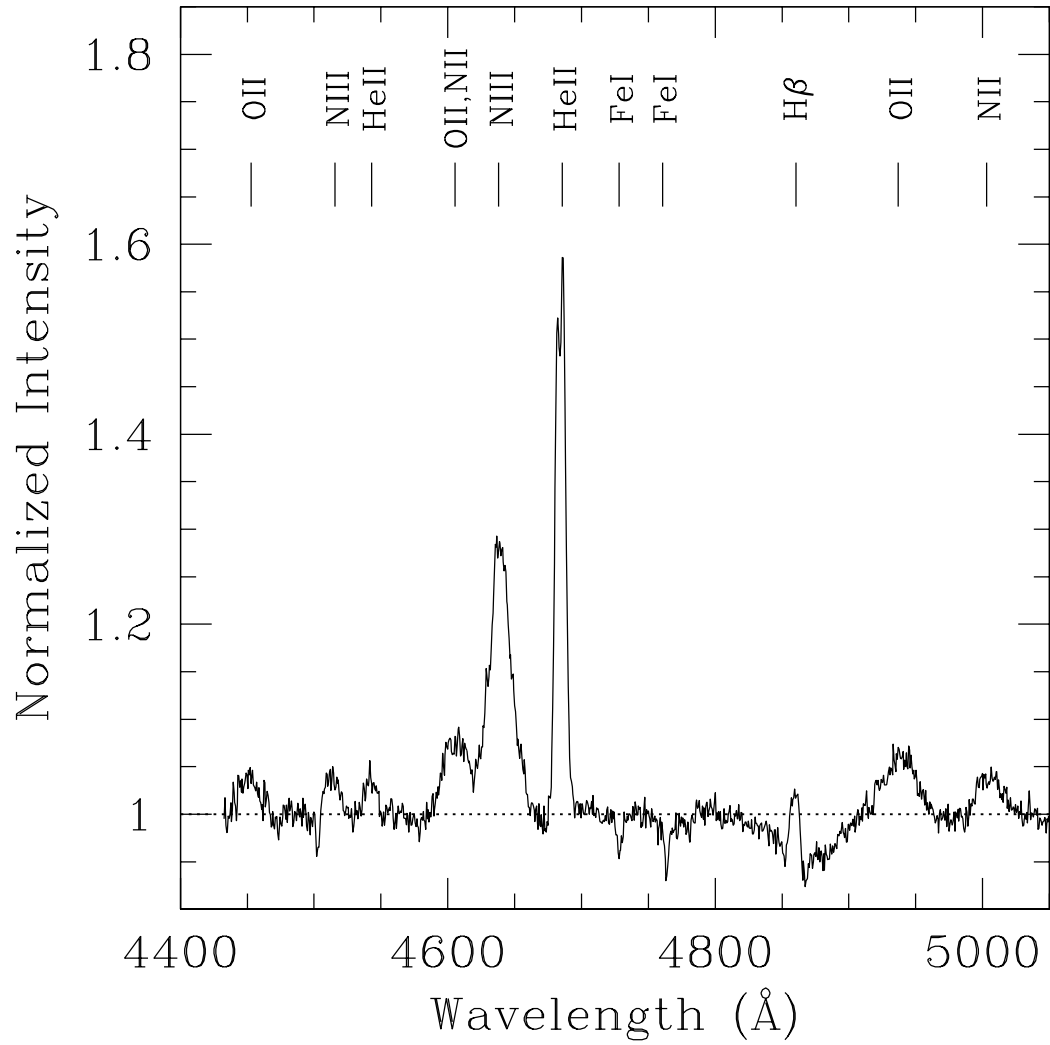


Fig. 16.— Averaged blue spectrum obtained by combining the spectra taken from 1994 August 30 to September 4. Wavelengths are vacuum heliocentric and the intensity is normalized to the continuum. The most prominent features in the spectrum are marked. We notice the presence of broad absorption, broad (flat-topped) emission and narrow emission lines.

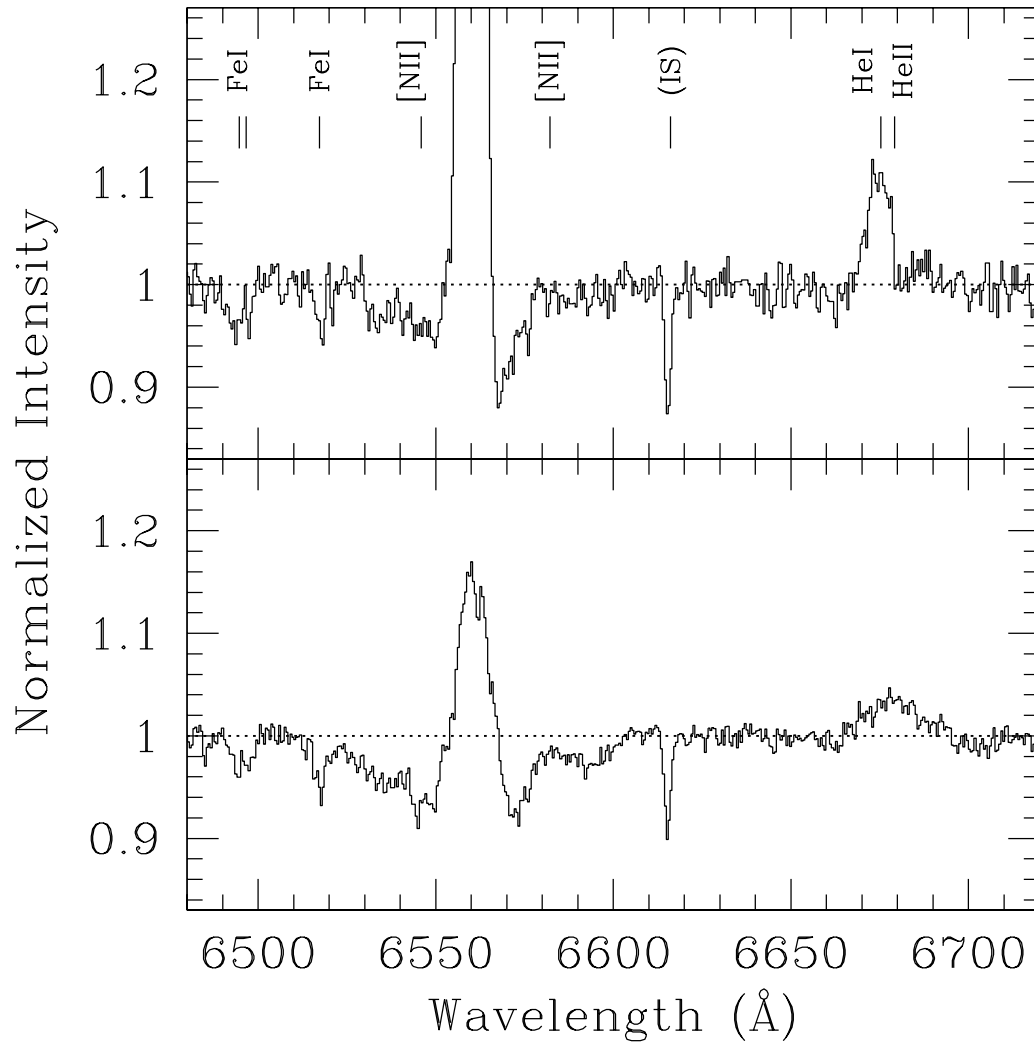


Fig. 17.— Top panel: expanded view of the H α region in the normalized spectrum from August 30. Bottom panel: expanded view of the same region in the normalized, combined spectrum from August 31 and September 1. The narrow emission components at H α and He I λ 6678 were much stronger on August 30 than on the following two days.

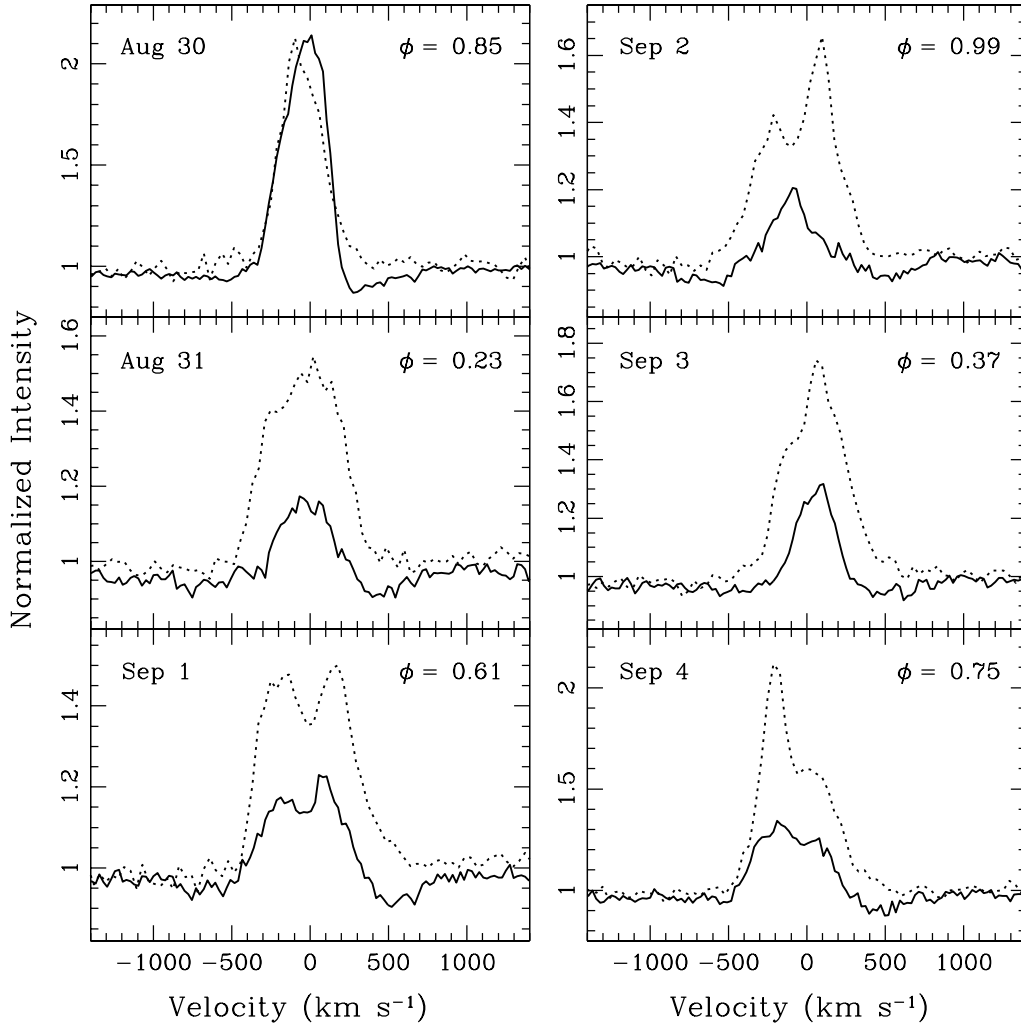


Fig. 18.— H α (solid curves) and He II $\lambda 4686$ (dashed curves) line profiles observed between 1994 August 30 and September 4. A red and a blue spectrum were taken in succession on each night. The phase indicated in each diagram refers to the observations of H α ; the phases of He II $\lambda 4686$ are $\phi_{H\alpha} + 0.01$. He II $\lambda 4686$ appeared generally broader than H α , an indication that the line was emitted at smaller radii or closer to the disk plane. Both lines showed transitions between a single-peaked and a double-peaked kind of profile. The velocity zeropoint is here the systemic velocity, -142.4 km s^{-1} . On average, both lines were blueshifted with respect to the systemic velocity; see §6.5.

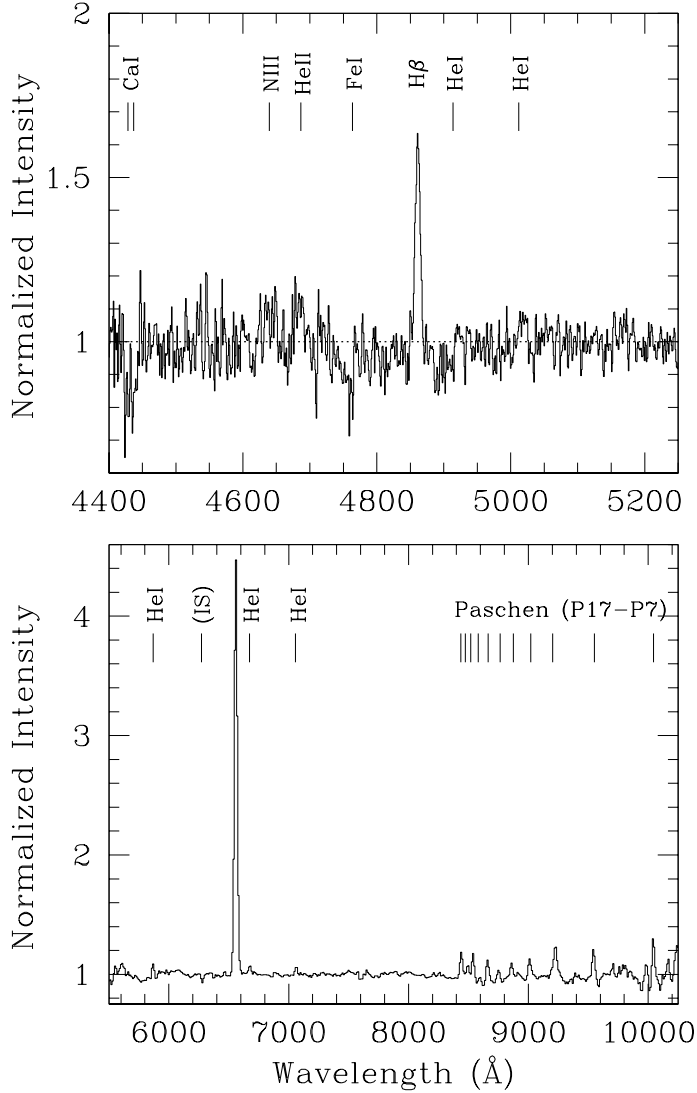


Fig. 19.— Top panel: medium-resolution blue spectrum obtained on 1994 September 6. Bottom panel: low-resolution red spectrum obtained at the same time. Wavelengths are vacuum heliocentric and the intensity is normalized to the continuum. The flat-topped metal emission lines and the broad Balmer absorption troughs observed in the previous nights had disappeared. High-ionization lines such as He II and Bowen N III had become much weaker; cf. Figure 16. The narrow $H\beta$ emission line had become stronger, but the $H\alpha/H\beta$ EW ratio had also increased dramatically. The H I Paschen lines were seen in emission. The dramatic change in the optical spectrum between September 4 and 6 coincided with a surge in the 20 – 100 keV X-ray flux measured by BATSE, and was followed by a major ejection of radio-emitting plasma on September 9.

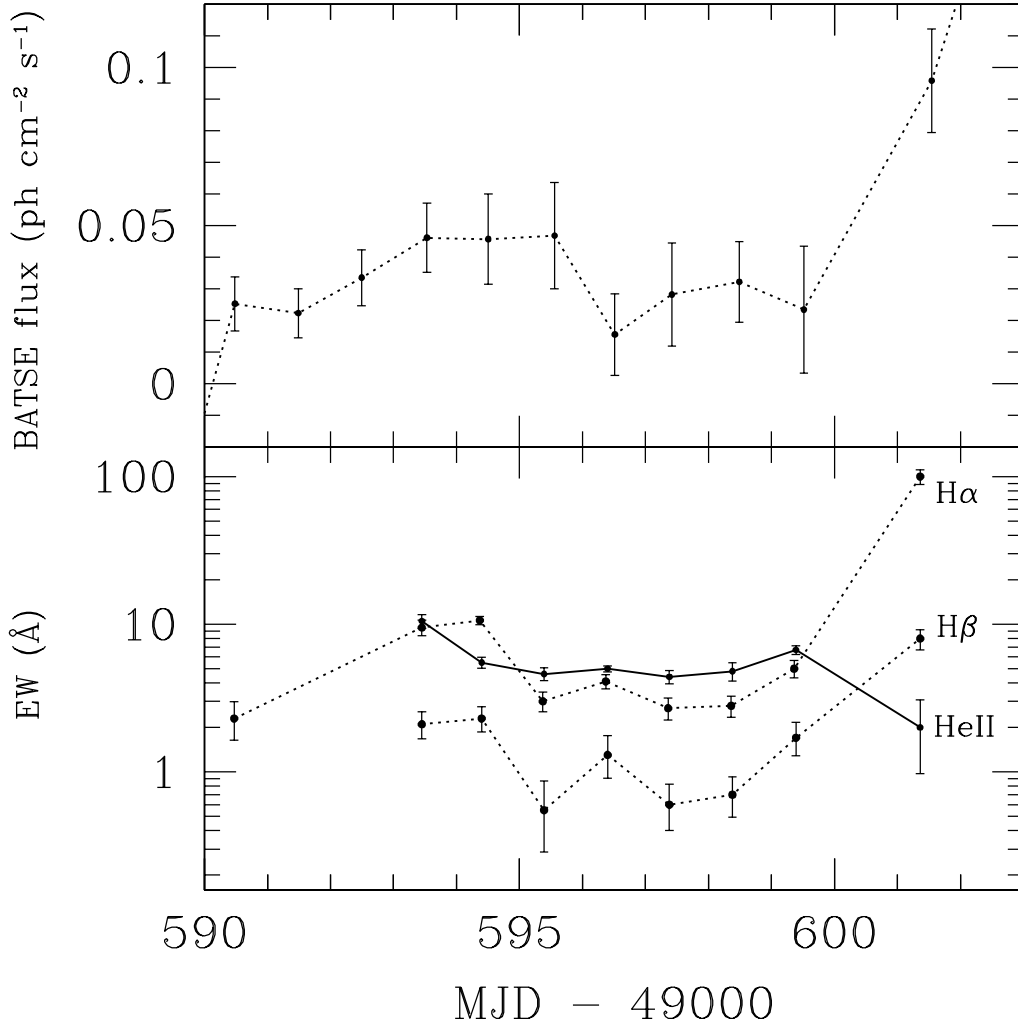


Fig. 20.— Top panel: hard (20–100 keV) X-ray flux, measured by BATSE during our 1994 August–September observations. Bottom panel: equivalent width of the H α , H β and He II λ 4686 emission lines during the same epoch. The EW of H α on MJD 49601.36 (September 6) was 100 ± 5 Å, a factor of 20 stronger than on the previous nights. A similar correlation between H α emission and hard X-ray flux was observed in 1996 June. The EW of H α on MJD 49590.47 has been determined from a spectrum taken for us on August 26 by Gary Da Costa. The values of EW on MJD 49593.47 have been obtained from a spectrum taken for us on August 29 by Raffaella Morganti.

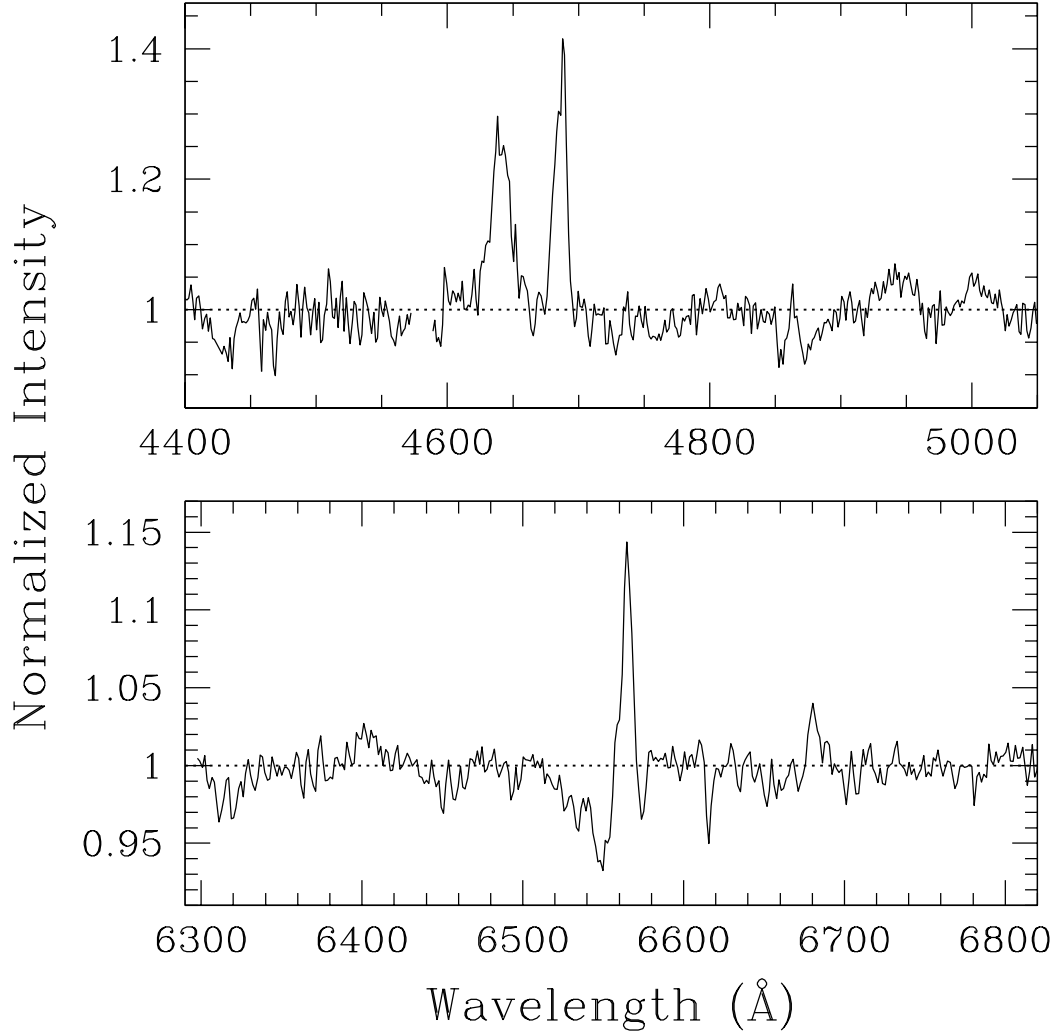


Fig. 21.— Top panel: medium-resolution blue spectrum taken with the 3.9 m Anglo-Australian Telescope on 1994 September 27 (HJD 2449622.867 = MJD 49622.367). Bottom panel: medium-resolution red spectrum from the same night (HJD 2449622.902 = MJD 49622.402). These spectra, obtained from the AAT archive, show that two weeks after the end of the hard X-ray flare (cf. Figure 2 in Hjellming 1997) the system had returned to a state very similar to the one we observed before September 5. Cf. Figures 15 and 16 for an identification of the main features.